Cross-code comparison of the edge codes SOLPS-ITER, SOLEDGE2D and UEDGE in modelling a low-power scenario in the DTT

Cross-code Comparison of the Edge Codes SOLPS-ITER, SOLEDGE2D and UEDGE in Modelling a Low-power Scenario in the DTT

M. Moscheni[1], C. Meineri[1], M. Wigram[2], C. Carati[3], E. De Marchi[3], M. Greenwald[2], P. Innocente[4], B. LaBombard[2], F. Subba[1], H. Wu[1], and R. Zanino[1]

[1] *NEMO Group, Dipartimento Energia, Politecnico di Torino, Corso Duca degli Abruzzi 24, 10129, Torino, Italy*
[2] *MIT Plasma Science and Fusion Center, Cambridge, MA 02139, USA*
[3] *Eni S.p.A., Italy*
[4] *Consorzio RFX, corso Stati Uniti, 4, Padova, Italy*

Abstract

As reactor-level nuclear fusion experiments are approaching, a solution to the power exhaust issue in future fusion reactors is still missing. The maximum steady-state heat load that can be exhausted by the present technology is around 10 MW/m^2. Different promising strategies aiming at successfully managing the power exhaust in reactor-relevant conditions such that the limit is not exceeded are under investigation, and will be tested in the Divertor Tokamak Test (DTT) experiment. Meanwhile, the design of tokamaks beyond the DTT, e.g. EU-DEMO/ARC, is progressing at a high pace. A strategy to work around the present lack of reactor-relevant data consists of exploiting modelling to reduce the uncertainty in the extrapolation in the design phase. Different simulation tools, with their own capabilities and limitations, can be employed for this purpose. In this work, we compare SOLPS-ITER, SOLEDGE2D and UEDGE, three state-of-the-art edge codes heavily used in power exhaust studies, in modelling the same DTT low-power, pure-deuterium, narrow heat-flux-width scenario. This simplified, although still reactor-relevant, testbed eases the cross-comparison and the interpretation of the code predictions, to identify areas where results differ and develop understanding of the underlying causes. Under the conditions investigated, the codes show encouraging agreement in terms of key parameters at both targets, including peak parallel heat flux (1-45%), ion temperature (2-19%), and inner target plasma density (1-23%) when run with similar input. However, strong disagreement is observed for the remaining quantities, from 30% at outer mid-plane up to a factor 4-5 at the targets. The results primarily reflect limitations of the codes: the SOLPS-ITER plasma mesh not reaching the first wall, SOLEDGE2D not including ion-neutral temperature equilibration, and UEDGE enforcing a common ion-neutral temperature. Potential improvements that could help enhance the accuracy of the code models for future applications are also discussed.

Keywords: DTT, scrape-off layer, power exhaust, edge modelling, SOLPS-ITER, SOLEDGE2D, UEDGE

E-mail of corresponding author: *matteo.moscheni@polito.it*

1 Introduction

The overarching goal to be achieved by nuclear fusion research is the practical demonstration of the feasibility of net, safe and economically viable electricity production [1]. Along with the mainstream fusion reactor concepts based on large-size, low-aspect-ratio tokamaks (e.g. the EU-DEMO [2]), alternative designs of compact reactors with high magnetic field (e.g. ARC [3]) are being developed. Regardless of the approach adopted, the problems of power exhaust are some of the major open issues still to be solved to demonstrate that a fusion energy plant is feasible [1].

In a conventional reactor concept, a few hundred MW of power exhaust flows from the core plasma into the Scrape-Off-Layer (SOL). Projections of the energy transport in the SOL suggest that the SOL radial extension (quantified by the power decay length λ_q) remains extremely narrow, on the order of millimeters [4]. Although the more recent [5] points towards a plasma-turbulence-driven widening of λ_q, this still results in a tiny wetted area $A < 1\ \mathrm{m}^2$ on the divertor, where $A \propto \lambda_q \cdot 2\pi R$ and R being the tokamak major radius. Under such circumstances, the current strategy, capable of exhausting $\sim$10 $\mathrm{MW/m}^2$ at most [6][7], would fall short of its objective. Therefore, several strategies, among which liquid metal divertors [8], SOL magnetic topology shaping to increase the wetted area [9][10] and impurity seeding aimed at stimulating radiation losses [11][12], are being investigated. At the present stage, the extrapolation of such ideas to next-step devices via SOL plasma modelling relies on, and is limited by, the current availability of reactor-relevant experimental data.

The flexible Divertor Tokamak Test (DTT) experiment [13], which will address the tokamak power exhaust problem, is currently under construction in Italy to test, in reactor-relevant conditions scaled to ITER, the aforementioned innovative divertor concepts. The newly-gathered experimental data will support the design of future reactors, and validation studies of the SOL simulation codes will reduce the modelling uncertainty. However, due to different levels of sophistication of the physics models within the modern edge plasma modelling tools, the reliability of extrapolations to future devices will still partially depend on the particular code selected. It is therefore necessary to understand how the differences among the models and numerics implemented by the different codes impact their own predictions.

In this paper, we present a quantitative comparison of the results of three of the most popular edge codes, namely SOLPS-ITER [14], SOLEDGE2D [15] and UEDGE [16], in simulating a DTT low-power pure-D plasma scenario, using commonly employed settings for each code. The simplified scenario assumptions of low power and no seeding, although still representative of the DTT experiment and relevant for future reactors (because of the small λ_q), are chosen to ease the comparison and the interpretation of the results. This assessment demonstrates how the different code-specific capabilities and limitations impact on the output, and suggests possible code improvements that will enhance the fidelity of future simulations, similarly to what has been accomplished in [17]. Moreover, it constitutes a basis of understanding on which future work involving impurity seeding and detached divertor, in the fashion of the currently ongoing [18], and code comparison against experimental data, as in [19], will build.

The paper is organised as follows. In Section 2, the plasma, neutral and transport models employed by the three codes are commented on and compared. In Section 3, the input for the simulation of the DTT reference scenario is discussed, consisting of the different code-specific meshes adopted, the boundary conditions, the transport and the neutrals-related parameters. In Section 4, the simulation results obtained by the three codes are presented, and the level of disagreement with each other is quantified. Section 5 discusses how these results can originate from the coding differences and from the physics models implemented. Finally, Section 6 outlines the main conclusions and perspective of this work.

2 Simulation codes: SOLPS-ITER, SOLEDGE2D, UEDGE

2.1 Plasma models

Coherently with the aforementioned aim of easing the cross-code comparison and result interpretation, a pure D plasma is considered. Drifts and electric currents are also neglected, for the sake of simplicity. With all the three codes relying on a multi-fluid approach for the plasma in a toroidally symmetric domain [20][21], the plasma becomes a mixture of different fluid charged species. For each species, the particle, momentum and energy transport are solved.

For the detailed set of equations solved by each code, the reader is referred to [14] for SOLPS-ITER (version 3.0.6), [15] for SOLEDGE2D (latest version), and [22] for UEDGE (version 7.06).
This section shows that the physics models implemented in the three codes are sufficiently close to allow a well-posed cross-code comparison. Minor differences are analysed in Section 5.1.

2.1.1 Continuity equation

The continuity equation (particle conservation) for the generic ionic species reads:

$$\frac{\partial n_\mathrm{i}}{\partial t} + \nabla \cdot (n_\mathrm{i} \mathbf{V}_\mathrm{i}) = S^n_\mathrm{i} \tag{1}$$

for all the codes, where n_i and $\mathbf{V}_\mathrm{i}$ are the plasma density and flow velocity respectively. The volumetric net particle source S^n_i includes different processes driven by ion-electron and plasma-neutral interactions. Discrepancies and similarities among the codes in S^n_i, in the momentum S^m_i, ion energy S^E_i and electron energy S^E_e sources are commented in detail in Section 2.2.

2.1.2 Parallel momentum equations

The component parallel ($\|$) to the magnetic field (B) of the momentum equation for the generic ionic species is solved by each code [23]. While SOLEDGE2D and UEDGE adopt the same formulation, SOLPS-ITER includes additional terms. The SOLPS-ITER equation specifically reads:

$$\begin{aligned}
&\frac{\partial}{\partial t}(m_\mathrm{i} n_\mathrm{i} V_{\mathrm{i}\|}) + \frac{\partial}{\partial x}\left[m_\mathrm{i} n_\mathrm{i} V_{\mathrm{i}\|}\left(b_x V_{\mathrm{i}\|} + V^{\mathrm{diff}}_{\mathrm{i}x,n} + V^{\mathrm{corr}}_{\mathrm{i}x}\right) - \left(\eta^{\mathrm{CL}}_{\mathrm{i}x} + \eta^{\mathrm{AN}}_\mathrm{i}\right)\frac{\partial V_{\mathrm{i}\|}}{\partial x} + \eta^{\mathrm{CL}}_{\mathrm{i}x} V_{\mathrm{i}\|}\frac{\partial \ln h_z}{\partial x}\right] + \\
&\frac{\partial}{\partial y}\left[m_\mathrm{i} n_\mathrm{i} V^{\mathrm{diff}}_{\mathrm{i}y,n} - \eta^{\mathrm{AN}}_\mathrm{i}\frac{\partial V_{\mathrm{i}\|}}{\partial y}\right] = -b_x\frac{\partial\left(p_\mathrm{i}+p_\mathrm{e}\right)}{\partial x} + \frac{\partial}{\partial x}\left[\frac{\eta^{\mathrm{CL}}_{\mathrm{i}x}}{\sqrt{B}}\frac{\partial\left(h_z\sqrt{B}\right)}{\partial x}\right]\sqrt{B}V_{\mathrm{i}\|} + S^m_\mathrm{i}
\end{aligned} \tag{2}$$

while that of SOLEDGE2D and UEDGE:

$$\frac{\partial}{\partial t}(m_\mathrm{i} n_\mathrm{i} V_{\mathrm{i}\|}) + \frac{\partial}{\partial x}\left[m_\mathrm{i} n_\mathrm{i} V_{\mathrm{i}\|} b_x V_{\mathrm{i}\|} - \eta^{\mathrm{CL}}_{\mathrm{i}x}\frac{\partial V_{\mathrm{i}\|}}{\partial x}\right] + \frac{\partial}{\partial y}\left[m_\mathrm{i} n_\mathrm{i} V^{\mathrm{diff}}_{\mathrm{i}y,n} - \eta^{\mathrm{AN}}_\mathrm{i}\frac{\partial V_{\mathrm{i}\|}}{\partial y}\right] = -b_x\frac{\partial\left(p_\mathrm{i}+p_\mathrm{e}\right)}{\partial x} + S^m_\mathrm{i} \tag{3}$$

where x, y and z are the poloidal, radial (i.e., across flux surfaces) and toroidal coordinates, respectively, $b_x = B_x/B$, $\eta^{\mathrm{CL}}_{\mathrm{i}x}$ and $\eta^{\mathrm{AN}}_\mathrm{i}$ are the classical and anomalous plasma viscosities, m_i is the ion mass, $\mathbf{V}^{\mathrm{diff}}_{\mathrm{i},n} = [V^{\mathrm{diff}}_{\mathrm{i}x,n}\,;\, V^{\mathrm{diff}}_{\mathrm{i}y,n}] = -D^{\mathrm{AN}}/n_\mathrm{i}[\partial_x n_\mathrm{i}\,;\,\partial_y n_\mathrm{i}]$ is the particle-driven diffusive velocity, and p_i and p_e are the ion and electron pressures. The term $b_x\partial_x p_\mathrm{e}$ follows from assuming the electrons to be inertialess in all the codes, hence replacing the contribution of the electric ($\propto b_x E_x$) and thermal ($\propto \partial_x T_\mathrm{e}$) forces.
Absent in the other two codes, the SOLPS-ITER additional terms are found in: the poloidal component $V^{\mathrm{diff}}_{\mathrm{i}x,n}$ of the particle-driven diffusive velocity; $V^{\mathrm{corr}}_{\mathrm{i}x} \propto \sqrt{p_\mathrm{i}/(m_\mathrm{i} n_\mathrm{i})}\partial^2_x[(\partial_x p_\mathrm{i})/p_\mathrm{i}]$, a numerical damping term to avoid the checkerboard instability [14]; $\eta^{\mathrm{CL}}_{\mathrm{i}x} V_{\mathrm{i}\|}\partial_x(\ln h_z)$ and $\partial_x[\eta^{\mathrm{CL}}_{\mathrm{i}x}\partial_x(h_z\sqrt{B})/\sqrt{B}]\sqrt{B}V_{\mathrm{i}\|}$ originating from the adoption of field-aligned coordinates [24], which depend on the metric coefficient for the toroidal direction $h_z = 2\pi R$. These terms will be discussed in Section 5.1.

2.1.3 Ion energy equations

In the fluid models employed by the three codes, it is assumed that temperatures along the parallel and perpendicular directions are perfectly equilibrated [25][26]. Apart from further additional SOLPS-ITER terms similar to those in Section 2.1.2, the formulations of the three codes are equivalent.
The ion energy equation for SOLPS-ITER is given by:

$$\begin{aligned}
&\frac{\partial}{\partial t}\left(\frac{3}{2}n_\mathrm{i} T_\mathrm{i}\right) + \frac{\partial}{\partial x}\left[\frac{3}{2}n_\mathrm{i} T_\mathrm{i}\left(b_x V_{\mathrm{i}\|} + \frac{5}{3}V^{\mathrm{diff}}_{\mathrm{i}x,n} + V^{\mathrm{corr}}_{\mathrm{i}x}\right) - \left(\kappa^{\mathrm{CL}}_{\mathrm{i}x} + \kappa^{\mathrm{AN}}_\mathrm{i}\right)\frac{\partial T_\mathrm{i}}{\partial x}\right] + \\
&\frac{\partial}{\partial y}\left[\frac{5}{2}n_\mathrm{i} T_\mathrm{i} V^{\mathrm{diff}}_{\mathrm{i}y,n} - \kappa^{\mathrm{AN}}_\mathrm{i}\frac{\partial T_\mathrm{i}}{\partial y}\right] = -p_\mathrm{i}\frac{\partial\left(b_x V_{\mathrm{i}\|}\right)}{\partial x} + \left[\left(\eta^{\mathrm{CL}}_{\mathrm{i}x} + \eta^{\mathrm{AN}}_\mathrm{i}\right)\left(\frac{\partial V_{\mathrm{i}\|}}{\partial x}\right)^2 + \eta^{\mathrm{AN}}_\mathrm{i}\left(\frac{\partial V_{\mathrm{i}\|}}{\partial y}\right)^2\right] + S^E_\mathrm{i}
\end{aligned} \tag{4}$$

For SOLEDGE2D:

$$\frac{\partial}{\partial t}\left(\frac{3}{2}n_{\mathrm{i}}T_{\mathrm{i}}+\frac{1}{2}m_{\mathrm{i}}n_{\mathrm{i}}\left|\mathbf{V}_{\mathrm{i}}\right|^{2}\right)+\frac{\partial}{\partial x}\left[\left(\frac{5}{2}n_{\mathrm{i}}T_{\mathrm{i}}+\frac{1}{2}m_{\mathrm{i}}n_{\mathrm{i}}\left|\mathbf{V}_{\mathrm{i}}\right|^{2}\right)b_{x}V_{\mathrm{i}\parallel}-\kappa_{\mathrm{i}x}^{\mathrm{CL}}\frac{\partial T_{\mathrm{i}}}{\partial x}\right]+$$
$$\frac{\partial}{\partial y}\left[\left(\frac{5}{2}n_{\mathrm{i}}T_{\mathrm{i}}+\frac{1}{2}m_{\mathrm{i}}n_{\mathrm{i}}\left|\mathbf{V}_{\mathrm{i}}\right|^{2}\right)V_{\mathrm{i}y,n}^{\mathrm{diff}}-\kappa_{\mathrm{i}}^{\mathrm{AN}}\frac{\partial T_{\mathrm{i}}}{\partial y}\right]=-p_{\mathrm{i}}\frac{\partial\left(b_{x}V_{\mathrm{i}\parallel}\right)}{\partial x}+\left[\frac{1}{2}\eta_{\mathrm{i}x}^{\mathrm{CL}}\frac{\partial V_{\mathrm{i}\parallel}^{2}}{\partial x}+\frac{1}{2}\eta_{\mathrm{i}}^{\mathrm{AN}}\frac{\partial V_{\mathrm{i}\parallel}^{2}}{\partial y}\right]+S_{\mathrm{i}}^{E} \tag{5}$$

And for UEDGE:

$$\begin{aligned}&\frac{\partial}{\partial t}\left(\frac{3}{2}n_{\mathrm{i}}T_{\mathrm{i}}\right)+\frac{\partial}{\partial x}\left[\frac{5}{2}n_{\mathrm{i}}T_{\mathrm{i}}b_{x}V_{\mathrm{i}\parallel}-\kappa_{\mathrm{i}x}^{\mathrm{CL}}\frac{\partial T_{\mathrm{i}}}{\partial x}\right]+\frac{\partial}{\partial y}\left[\frac{5}{2}n_{\mathrm{i}}T_{\mathrm{i}}V_{\mathrm{i}y,n}^{\mathrm{diff}}-\kappa_{\mathrm{i}}^{\mathrm{AN}}\frac{\partial T_{\mathrm{i}}}{\partial y}\right]\\&=\mathbf{V}_{\mathrm{i}}\cdot\nabla p_{\mathrm{i}}+\left[\eta_{\mathrm{i}x}^{\mathrm{CL}}\left(\frac{\partial V_{\mathrm{i}\parallel}}{\partial x}\right)^{2}+\eta_{\mathrm{i}}^{\mathrm{AN}}\left(\frac{\partial V_{\mathrm{i}\parallel}}{\partial y}\right)^{2}\right]+S_{\mathrm{i}}^{E}\end{aligned} \tag{6}$$

where $\kappa_{\mathrm{i}x}^{\mathrm{CL}}$ and $\kappa_{\mathrm{i}}^{\mathrm{AN}}$ are the classical and anomalous ion heat conductivities, respectively, and T_{i} is the ion temperature. The SOLPS-ITER and UEDGE internal energy equations are very similar, although UEDGE features a Right-Hand Side (RHS) term in $\mathbf{V}_{\mathrm{i}}\cdot\nabla p_{\mathrm{i}}$ rather than $-p_{\mathrm{i}}\partial_{x}\left(b_{x}V_{\mathrm{i}\parallel}\right)$, and the factor $5/2$ replaces the $3/2$ in the UEDGE Left-Hand Side (LHS) x-flux term. Instead, the total energy balance is solved in SOLEDGE2D. Still, the three formulations are mathematically equivalent.
It should be noted that UEDGE, when running with its full fluid neutral model, has the capability to add a corresponding atom temperature equation to Eq. 6, and in this setup the form of the ion energy equation solves for a mean ion-atom temperature. However, in this work the simpler diffusive neutral model is employed (discussed further in Section 2.2), and so the formulation given in Eq. 6 is used, with the assumption taken for the atom temperature $T_{\mathrm{g}}=T_{\mathrm{i}}$.

2.1.4 Electron energy equations

The electron energy equations closely resemble those for the ions. The detailed expression for the electron energy conservation is, for SOLPS-ITER:

$$\frac{\partial}{\partial t}\left(\frac{3}{2}n_{\mathrm{e}}T_{\mathrm{e}}\right)+\frac{\partial}{\partial x}\left[\frac{3}{2}n_{\mathrm{e}}T_{\mathrm{e}}\left(b_{x}V_{\mathrm{e}\parallel}+\frac{5}{3}V_{\mathrm{e}x,n}^{\mathrm{diff}}+V_{\mathrm{e}x}^{\mathrm{corr}}\right)-\left(\kappa_{\mathrm{e}x}^{\mathrm{CL}}+\kappa_{\mathrm{e}}^{\mathrm{AN}}\right)\frac{\partial T_{\mathrm{e}}}{\partial x}\right]+$$
$$\frac{\partial}{\partial y}\left[\frac{5}{2}n_{\mathrm{e}}T_{\mathrm{e}}V_{\mathrm{e}y,n}^{\mathrm{diff}}-\kappa_{\mathrm{e}}^{\mathrm{AN}}\frac{\partial T_{\mathrm{e}}}{\partial y}\right]=-p_{\mathrm{e}}\frac{\partial\left(b_{x}V_{\mathrm{e}\parallel}\right)}{\partial x}+S_{\mathrm{e}}^{E} \tag{7}$$

For SOLEDGE2D:

$$\frac{\partial}{\partial t}\left(\frac{3}{2}n_{\mathrm{e}}T_{\mathrm{e}}\right)+\frac{\partial}{\partial x}\left[\frac{5}{2}n_{\mathrm{e}}T_{\mathrm{e}}b_{x}V_{\mathrm{e}\parallel}-\kappa_{\mathrm{e}x}^{\mathrm{CL}}\frac{\partial T_{\mathrm{e}}}{\partial x}\right]+\frac{\partial}{\partial y}\left[\frac{5}{2}n_{\mathrm{e}}T_{\mathrm{e}}V_{\mathrm{e}y,n}^{\mathrm{diff}}-\kappa_{\mathrm{e}}^{\mathrm{AN}}\frac{\partial T_{\mathrm{e}}}{\partial y}\right]=-p_{\mathrm{e}}\frac{\partial\left(b_{x}V_{\mathrm{e}\parallel}\right)}{\partial x}+S_{\mathrm{e}}^{E} \tag{8}$$

And for UEDGE:

$$\begin{aligned}&\frac{\partial}{\partial t}\left(\frac{3}{2}n_{\mathrm{e}}T_{\mathrm{e}}\right)+\frac{\partial}{\partial x}\left[\frac{5}{2}n_{\mathrm{e}}T_{\mathrm{e}}b_{x}V_{\mathrm{e}\parallel}-\kappa_{\mathrm{e}x}^{\mathrm{CL}}\frac{\partial T_{\mathrm{e}}}{\partial x}\right]+\frac{\partial}{\partial y}\left[\frac{5}{2}n_{\mathrm{e}}T_{\mathrm{e}}V_{\mathrm{e}y,n}^{\mathrm{diff}}-\kappa_{\mathrm{e}}^{\mathrm{AN}}\frac{\partial T_{\mathrm{e}}}{\partial y}\right]\\&=\left[b_{x}V_{\mathrm{i}\parallel}\frac{\partial p_{\mathrm{e}}}{\partial x}-V_{\mathrm{i}y,n}^{\mathrm{diff}}\frac{\partial p_{\mathrm{i}}}{\partial y}\right]+S_{\mathrm{e}}^{E}\end{aligned} \tag{9}$$

where $\kappa_{\mathrm{e}x}^{\mathrm{CL}}$ and $\kappa_{\mathrm{e}}^{\mathrm{AN}}$ are the classical and anomalous electron heat conductivities, respectively, and T_{e} is the electron temperature. In SOLEDGE2D and UEDGE the source term S_{e}^{E} is redefined so that the general form of the equation is equivalent to that of SOLPS-ITER: the factor $5/2$ in the LHS fluxes is retained, and UEDGE employs the energy variation due to the pressure-gradient force while SOLPS-ITER and SOLEDGE2D retain the $-p_{\mathrm{e}}\partial_{x}(b_{x}V_{\mathrm{e}\parallel})$ term.

2.2 Neutral models, reactions and source terms

For the neutral particles, SOLPS-ITER and SOLEDGE2D rely on the coupling with EIRENE [27], a Monte Carlo (MC) code implementing a kinetic model capable of accounting for a large number of processes, including Electron Ionization (EI), ReCombination (RC), Charge eXchange (CX) and non-resonant ELastic collisions[1] (EL) of D atoms, D_2 molecules and, despite being a charged species, D_2^+ molecular ions. D_2 and D_2^+ DiSsociation (DS) is also accounted for.
More specifically, for each process (P), different reaction branches (r) are allowed, and the reactivity of each such reactions $\langle\sigma v\rangle_{P,r}$ [$m^3 \cdot s^{-1}$] is obtained by averaging the cross section σ in the velocity space [28]. EIRENE requires $\langle\sigma v\rangle_{P,r}$ to be expressed via a polynomial fit depending on 1 (ion temperature) or 2 [ion temperature and (ion density or neutral energy)] parameters, with a corresponding reaction-dependent range of validity [29][30] (Section 5.5). By default, while SOLPS-ITER implements 17 processes, 12 are considered by SOLEDGE2D. Of these 17 (12) reactions of SOLPS-ITER (SOLEDGE2D) listed in Table 1, 11 (9) are strictly involved in the computation of reactivities $\langle\sigma v\rangle_{P,r}$. Instead, the other 6 (3) employ fits: for energy-weighted reactivites (ϟ in Table 1) entering the energy sources (see below); for cross sections σ as a function of the energy in the laboratory reference frame (†); and for EL interaction potential (‡). Then, if the r^{th} (binary) reaction involves the species a and b, the corresponding source/sink reads $S_{P,r} = \pm n_r^a n_r^b \langle\sigma v\rangle_{P,r}$, in such a way that $S_P = \sum_r S_{P,r}$. The consequences of having the two codes employ by default different reactions (bold and entries left blank in Table 1) are investigated in Section 5.5 and 5.6.

Process (P)	Reaction (r)			SOLPS-ITER			SOLEDGE2D		
EI	$e + D$	$\rightarrow$	$2e + D^+$	AMJ	H.4	2.1.5	AMJ	H.4	2.1.5
				AMJ	H.10	2.1.5 (ϟ)	AMJ	H.10	2.1.5 (ϟ)
	$e + D_2$	$\rightarrow$	$2e + D_2^+$	AMJ	H.4	2.2.9	**HYD**	**H.2**	2.2.9
	$e + D_2^+$	$\rightarrow$	$2e + 2D^+$	AMJ	H.4	2.2.11	**HYD**	**H.2**	2.2.11
DS	$e + D_2$	$\rightarrow$	$e + 2D$	AMJ	H.4	2.2.5g	**HYD**	**H.2**	**2.2.5**
	$e + D_2$	$\rightarrow$	$2e + D + D^+$	AMJ	H.4	2.2.10	**HYD**	**H.2**	2.2.10
	$e + D_2^+$	$\rightarrow$	$e + D + D^+$	AMJ	H.4	2.2.12	**HYD**	**H.2**	2.2.12
	$e + D_2^+$	$\rightarrow$	$2D$	AMJ	H.4	2.2.14	**HYD**	**H.2**	2.2.14
	$e + D_2^+(\nu)$	$\rightarrow$	$D + D^*(n)$	AMJ	H.8	2.2.14 (ϟ)	AMJ	H.8	2.2.14 (ϟ)
CX	$D^+ + D$	$\rightarrow$	$D + D^+$	HYD	H.1	3.1.8 (†)		–	
				HYD	H.3	3.1.8	**AMJ**	**H.2**	**3.1.8FJ**
	$D^+ + D_2$	$\rightarrow$	$D + D_2^+$	AMJ	H.2	3.2.3		–	
EL	$D^+ + D_2$	$\rightarrow$	$D^+ + D_2$	AMJ	H.0	0.3T (‡)		–	
				AMJ	H.1	0.3T (†)		–	
				AMJ	H.3	0.3T		–	
RC	$D^+ + e$	$\rightarrow$	D	AMJ	H.4	2.1.8	AMJ	H.4	2.1.8
				AMJ	H.10	2.1.8 (ϟ)	AMJ	H.10	2.1.8 (ϟ)

Table 1: Default set of EIRENE reactions employed by SOLPS-ITER and SOLEDGE2D. Data are taken from the AMJUEL (AMJ) [29] or HYDHEL (HYD) [30] databases. Bolded and blank entries highlight differences between the reactivities. Symbols: ϟ = energy-weighted reactivity $\langle\sigma v\rangle$; † = fit for cross section σ as a function of the energy in the laboratory reference frame; ‡ = fit for interaction potential in elastic collisions.

[1] Atom-ion EL collisions are implicitly included in the atom-ion CX reactions due to the indistinguishability of the two processes from a quantum standpoint.

The overall net source entering Eq. 1 then reads:

$$S_{\mathrm{i}}^{n} = \sum_{P} S_P = S_{\mathrm{EI}}^{\mathrm{Eir}} + S_{\mathrm{RC}}^{\mathrm{Eir}} + S_{\mathrm{DS}}^{\mathrm{Eir}} = S_{\mathrm{D}}^{\mathrm{Eir}} + S_{\mathrm{D_2}}^{\mathrm{Eir}} + S_{\mathrm{D_2^+}}^{\mathrm{Eir}} \tag{10}$$

where the second and third equality result from grouping reactions as a function of their parent process and of the EIRENE reactant involved, respectively. Notice that atomic CX (in SOLPS-ITER and SOLEDGE2D), molecular CX and EL (in SOLPS-ITER only) do not enter Eq. 10 not being a net source/sink of particles.
With an analogous treatment, the momentum S_{i}^{m} (Eqs. 2 and 3), ion energy S_{i}^{E} (Eqs. 4 and 5) and electron energy S_{e}^{E} (Eqs. 7 and 8) sources are computed by EIRENE.
Due to the inclusion of multiple neutral species in SOLPS-ITER and SOLEDGE2D, physical quantities generally referring to neutrals (and not involving $\mathrm{D_2^+}$) will also be used:

$$n_{\mathrm{g}} = n_{\mathrm{D}} + 2n_{\mathrm{D_2}} \ , \ p_{\mathrm{g}} = p_{\mathrm{D}} + 2p_{\mathrm{D_2}} \ , \ T_{\mathrm{g}} = p_{\mathrm{g}}/n_{\mathrm{g}} \tag{11}$$

for an appropriate comparison with UEDGE. Caution is required when referring to any neutral temperatures because of the presence of well-defined and well-separated neutral temperature spectra [31]: "hot" ($\gg 2$ eV) neutrals arising from thermalisation with ions, "warm" (~ 2 eV) atoms created by molecular DS and "cold" (~ 0.1 eV) molecules thermalised with the walls (Section 3.2.2).
In the model employed in this work, UEDGE considers only neutral atoms ($n_{\mathrm{g}} = n_{\mathrm{D}}$, $p_{\mathrm{g}} = p_{\mathrm{D}}$ and $T_{\mathrm{g}} = T_{\mathrm{D}}$), treated as an additional fluid species and sharing the same temperature with the ions (justification of this latter assumption is discussed in Section 5.2). It is worth noting that this same assumption of ion-neutral common temperature is also employed by SOLPS-ITER when run with its fluid neutral model rather than the kinetic treatment provided by EIRENE [14].
The full fluid neutral model available in UEDGE employs a momentum equation equivalent to Eq. 3 for the neutral species, but in this work the simpler diffusive-neutral model is used [22], due to a failure of convergence of the full neutral model using the DTT target plate geometry (though fully converged solutions for similar tilted divertor-plate geometries have previously been obtained, e.g. for the FNSF device [32]).
In the following, UEDGE sources are referred to but, unless otherwise specified, they match those of SOLPS-ITER and SOLEDGE2D. The UEDGE net particle source reads:

$$S_{\mathrm{i}}^{n} = \sum_{P} S_P = S_{\mathrm{EI}}^{\mathrm{Deg2}} + S_{\mathrm{RC}}^{\mathrm{Deg2}} \tag{12}$$

In an equivalent manner to EIRENE, the EI and RC reactivities are computed by DEGAS2 (Deg2) [33] and expressed in terms of a fit as a function of plasma densities and temperatures. Since UEDGE does not include neutral molecules in this work, DS is absent.
The UEDGE atomic CX reactivity is given by an analytical function of the ion temperature [34]:

$$\langle \sigma v \rangle_{\mathrm{CX}} = 1.7 \cdot 10^{-14} \cdot (0.3\, T_{\mathrm{i}})^{0.333} \tag{13}$$

with $[T_{\mathrm{i}}] = \mathrm{eV}$. This does not enter Eq. 12 since it does not account for a net source/sink of charged particles. Still, CX, EI and RC all give a contribution to the UEDGE momentum source[2]:

$$S_{\mathrm{i}}^{m} = -(m_{\mathrm{i}} V_{\mathrm{i}\parallel} - m_{\mathrm{g}} V_{\mathrm{g}\parallel}) S_{\mathrm{CX}} + m_{\mathrm{g}} V_{\mathrm{g}\parallel} S_{\mathrm{EI}}^{\mathrm{Deg2}} - m_{\mathrm{i}} V_{\mathrm{i}\parallel} S_{\mathrm{RC}}^{\mathrm{Deg2}} \tag{14}$$

The UEDGE ion energy source is given by:

$$S_{\mathrm{i}}^{E} = K_{\mathrm{EQ}}(T_{\mathrm{e}} - T_{\mathrm{i}}) + \frac{1}{2} m_{\mathrm{i}} V_{\mathrm{i}\parallel}^2 S_{\mathrm{EI}}^{\mathrm{Deg2}} - \frac{1}{2} m_{\mathrm{i}} V_{\mathrm{i}\parallel}^2 S_{\mathrm{RC}}^{\mathrm{Deg2}} + \tilde{S}_{\mathrm{i}}^{E} \tag{15}$$

The terms on the RHS include (from left to right): electron-ion thermal equilibration, with $K_{\mathrm{EQ}} \propto n_{\mathrm{e}} n_{\mathrm{i}} T_{\mathrm{e}}^{-3/2} \ln \Lambda$ representing the rate of Coulomb energy exchange collisions; the energy source (sink)

[2] SOLPS-ITER inter-charged-species thermal and friction forces contributing to S_{i}^{m} on the plasma side are deactivated in the current modelling [14].

associated to ionization (recombination); the term $\tilde{S}_{\rm i}^{E}$ due the volumetric contribution from neutral beam injection and radio-frequency heating, neglected in the present study. An additional contribution for the CX-driven ion-neutral thermal equilibration $K_{\rm CX}(T_{\rm g}-T_{\rm i})$ is absent in this formulation of $S_{\rm i}^{E}$ for UEDGE, given the $T_{\rm g}=T_{\rm i}$ assumption. Instead, $K_{\rm CX}(T_{\rm D}-T_{\rm i})\propto S_{\rm CX}^{\rm Eir,D}(T_{\rm D}-T_{\rm i})$ appears in SOLEDGE2D and $\propto S_{\rm CX}^{\rm Eir,D}(T_{\rm D}-T_{\rm i})+S_{\rm CX}^{\rm Eir,D_2}(T_{\rm D_2}-T_{\rm i})$ in SOLPS-ITER, the latter also additionally including molecule-ion equilibration via EL $\propto S_{\rm EL}^{\rm Eir,D_2}(T_{\rm D_2}-T_{\rm i})$.
Finally,the electron energy source in UEDGE is given by:

$$S_{\rm e}^{E}=\mathbf{j}\cdot\mathbf{E}+\tilde{S}_{\rm e}^{E} \tag{16}$$

and takes into account, respectively, Joule heating and volumetric radiation energy sinks (see Section 4). Conversely with respect to SOLPS-ITER and SOLEDGE2D, UEDGE Joule heating includes both contributions along x and y directions. Since currents are neglected in this work, both j_xE_x and j_yE_y vanish, excluding differences among the codes in the current context.

2.2.1 Classical and anomalous transport

The closure of plasma (and neutral for UEDGE) fluid equations via transport coefficients can predict unphysically large fluxes along the poloidal direction x in conditions where kinetic effects are important (such as low plasma collisionality or steep gradients) [35]. Therefore, a kinetic correction is applied to the transport coefficients in terms of flux limiters.
In general terms, if $\tilde{\xi}_x^{\rm CL}$ is the classical transport coefficient along x, the actual coefficient employed by the three codes in the SOL reads:

$$\xi_x^{\rm CL}=\tilde{\xi}_x^{\rm CL}\left[1+\left|\frac{X^{\rm CL}}{\alpha F}\right|^{\beta}\right]^{-1/\beta} \tag{17}$$

where $\xi_x^{\rm CL}\in\{\eta_{ix}^{\rm CL}\ ;\ \kappa_{{\rm e},ix}^{\rm CL}\}$, $X^{\rm CL}\in\{-\eta_{ix}^{\rm CL}\partial_x V_{\rm i\|}\ ;\ -\kappa_{{\rm e},ix}^{\rm CL}\partial_x T_{\rm e,i}\}$ is the corresponding limited flux, $F\in\{p_{\rm i}\ ;\ n_{\rm e,i}T_{\rm e,i}^{3/2}m_{\rm e,i}^{1/2}\}$ is the limiting flux quantity (e.g. the "free streaming flux" for the energy transport), and α is the user-defined flux limit factor. Given the well-known influence of the flux limiters on the result of a simulation [36][37], common values are chosen for the comparison. The viscosity flux limit factor is chosen as $\alpha=0.5$ [31], whereas $\alpha=0.21$ is selected according to [38] for both the electron and ion heat flux. The exponent is set to $\beta=1$ in UEDGE to match the SOLPS-ITER and SOLEDGE2D expressions. Braginskii formulation is enforced in all the three codes when computing the classical transport coefficients $\tilde{\xi}_x^{\rm CL}$ [35].
In the simple diffusive neutral model, UEDGE flux-limits the atom particle and thermal flux in a similar manner to Eq. 17, with $F\in\{C_1n_{\rm g}v_{\rm g,th}\ ;\ C_2n_{\rm g}v_{\rm g,th}T_{\rm g}\}$ respectively, where $v_{\rm g,th}$ is the neutral thermal velocity and $\{C_1;C_2\}$ are constants, and typically $\alpha=1.0$.
For the anomalous radial transport of the plasma species, particles, momentum and energy are transported by turbulent processes: the codes assume these processes to be reasonably approximated by a diffusive model with user-selected anomalous diffusivities (Section 3.1).

3 Simulation setup

3.1 Scenario characterization and comparison of code meshes

The reference DTT scenario has a plasma current $I_{\rm p}=5.5$ MA, with an on-axis magnetic field $B_0=6.0$ T. The equilibrium employed in the mesh generation was computed by CREATE-NL [39]. Based on the DTT parameters in [13], the electron and ion anomalous heat transport coefficients (Section 2.2.1) are estimated as $\chi_{\rm e,i}^{\rm AN}=0.15\,{\rm m}^2/{\rm s}$ ($\kappa_{\rm e,i}^{\rm AN}=n_{\rm e,i}\chi_{\rm e,i}^{\rm AN}$) according to the 2-point model [31], then $D^{\rm AN}=\chi_{\rm e,i}^{\rm AN}/3=0.05\,{\rm m}^2/{\rm s}$ is assumed for particles as in [9]. Such low and uniform values lead to a reactor-relevant small λ_q (1.2-1.9 mm, in line with Eich scaling predictions [4]) which in turn results in a more challenging, but also more meaningful, comparison. It is worthwhile underlining that the turbulence-driven λ_q broadening

predicted[3] according to [5] amounts to only 20-40% for the present DTT scenario. Last, $\nu_{\mathrm{i}}^{\mathrm{AN}} = 1\ \mathrm{m}^2/\mathrm{s}$ ($\eta_{\mathrm{i}}^{\mathrm{AN}} = m_{\mathrm{i}} n_{\mathrm{i}} \nu_{\mathrm{i}}^{\mathrm{AN}}$) for momentum is assumed.

The meshes generated for the abovementioned equilibrium and used by the three codes are shown in Figure 1. The plasma mesh consists of quadrilateral non-orthogonal cells. In SOLPS-ITER and UEDGE, this computational domain does not reach out to the First Wall (FW), but is instead radially restricted in the SOL (1.6-1.8 cm in width at Outer Mid-Plane, OMP, measured from the separatrix) and Private Flux Region (PFR, 3.5-5.0 cm in width at targets, measured from the strike point) by artificial boundaries, represented by a selected magnetic surface which contacts the divertor targets at both ends. On the contrary, in SOLEDGE2D the plasma mesh covers the entire domain out to the first wall but, likewise with SOLPS-ITER and UEDGE, is artificially limited in the core ($\sim$ 3.0 cm in width at OMP, measured from the separatrix). These meshes are built as similar as possible (at least in the common part of the domain), with 96×36 cells along x and y respectively, and enhanced refinement across the separatrix (> 6 cells in $1\lambda_q$ at OMP SOL along y) and close to the targets ($\sim$ 1-mm cell width along x), i.e. in regions where steep gradients are expected. The SOLEDGE2D mesh is generated without the use of a magnetic flux smoothing function option available in the code, as this changed the location of the separatrix relative to the other codes, which was found to have a significant impact on the results obtained (see Appendix A for further discussions).

For the neutral gas, UEDGE adopts the same mesh as for the plasma. Instead, EIRENE in SOLPS-ITER and SOLEDGE2D employs a triangulation which extends out to the wall, allowing a detailed description of reflection-absorption as well as of the pumping system performance. The triangulation is refined in the proximity of the gas puff port (at OMP) for SOLPS-ITER and in the PFR for both SOLPS-ITER and SOLEDGE2D.

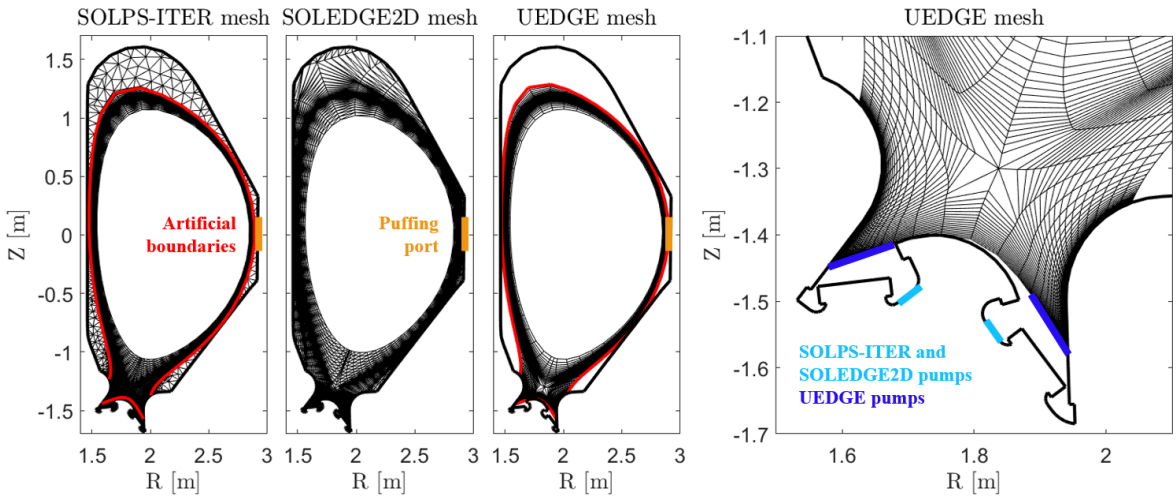

Figure 1: Meshes exploited by the three codes, from left to right: SOLPS-ITER (EIRENE), SOLEDGE2D (EIRENE), UEDGE, and zoomed-in UEDGE divertor region. The SOLPS-ITER and UEDGE artificial boundaries of the plasma (and neutral for UEDGE) domain are shown in red, and the outer midplane puffing port in amber. The actual DTT divertor pump locations on the vessel wall are considered by SOLPS-ITER and SOLEDGE2D (light blue), while UEDGE relies on artificial pumping surfaces on the private-flux region boundary (blue).

3.2 Boundary conditions and input parameters

3.2.1 Plasma fluid species

A particle influx of $5 \cdot 10^{20}$ D^+/s through the core boundary is specified for all codes. The Boundary Conditions (BCs) for the parallel ion momentum balance (Eqs. 2 and 3) consist of zero parallel velocity

[3]The plasma parameters are taken from Table 2 and [13], and the resulting turbulence parameter is $\alpha_t < 0.1$ [5].

at the core boundary and sound speed c_s at the sheath entrance ($\sim$ wall[4]) according to the Bohm criterion. The power P_{SOL} entering from the core boundary is set to 8 MW, equally shared between ion and electron *internal* energy equations. The electron energy sheath transmission coefficient γ_e appearing in the heat flux $\Gamma_e^E = \gamma_e n c_s T_e$ at the wall is set to 4.5 in all codes. For the ions, the SOLEDGE2D wall BC for the *total* energy equation reads $\Gamma_i^E = (\gamma_i T_i + m_i c_s^2/2) n_i c_s$, with the internal-energy sheath transmission coefficient $\gamma_i = 2.5$, hence matching that of SOLPS-ITER and UEDGE in $\Gamma_i^E = \gamma_i n_i c_s T_i$ for the *internal* energy.
In SOLPS-ITER and UEDGE, a decay-length of 3 cm is imposed at the artificial plasma boundaries for both density and temperature as in [40].
Secondary electron emission at the wall is neglected, according to [31], and the Coulomb logarithm is set to a constant value of 12.0 in all the codes, coherently with [41].

3.2.2 Neutrals

Neutrals are puffed in from the OMP wall (amber in Figure 1) at an equivalent[5] atomic deuterium puffing rate of $5 \cdot 10^{21}$ D/s. The size of the slot through which neutrals are puffed is similar among the codes despite being located on the OMP FW for SOLPS-ITER and SOLEDGE2D and on the outermost OMP cell side for UEDGE. In SOLPS-ITER, the slot then sits ~ 2 cm away from the outermost OMP cell along the SOL artificial boundary.
In regard to the wall properties, the temperature is set to $T_{wall} = 0.1$ eV and the material to "tungsten" in SOLPS-ITER and SOLEDGE2D. In UEDGE, the reflected/recycled neutrals are injected with energy of the local T_g at the mesh boundary. Recycling of neutral particles at the wall surface is enforced by setting the reflection coefficient, i.e. the albedo, $A_{wall} = 100\%$. Instead, the pump albedo $A_{pump} < 100\%$ is left as a free parameter to be adjusted independently for each code, although constraining it to realistic values for DTT ($A_{pump} > 98\% \Rightarrow$ flowrate $< 200\ m^3/s$ [13]). A common OMP separatrix density n_e^{SEP} is desired for the code-comparison, given the sensitivity of divertor solutions to the upstream density [19][31]. As such, A_{pump} is adjusted for each code such that the resulting plasma solution achieves a targeted $n_e^{SEP} = 5 \cdot 10^{19}\ m^{-3}$ (Section 4).

4 Results

Simulations of the DTT reference scenario outlined in Section 3 were to converge to steady-state solutions. Convergence criteria are different in the three codes: in SOLPS-ITER, according to [42] and [43], the evolution timescales of the output parameters are verified to be smaller than characteristic plasma ones; in SOLEDGE2D, total energy and particle balances are analyzed and then local values are checked to change no more than 1%; in UEDGE, the value of the normalized residuals of the Newton-Krylov solver must be below 10^{-10}, and a test for stationary conditions is performed by evolving a single time step with $\delta t \sim 10^{20}$ s.
The common targeted $n_e^{SEP} = 5 \cdot 10^{19}\ m^{-3}$ at the OMP (Section 3.2.2) is achieved by all the three codes within 2%. Due to the sensitivity of downstream conditions on upstream features [19][31], this choice allows a well-posed comparison between the codes.
Table 2 shows a concise summary of the main results in Figures from 2 to 4. With the indices $j, k \in$ {SOLPS-ITER; SOLEDGE2D; UEDGE}, for any output quantity of interest ζ (e.g. the peak density at the outer target):

$$\Delta \in \left[\min_{j \neq k} \{\Delta_{jk}\} \, ; \, \max_{j \neq k} \{\Delta_{jk}\} \right] \text{ with } \Delta_{jk} = \frac{|\zeta_j - \zeta_k|}{(\zeta_j + \zeta_k)/2} \cdot 100\ [\%] \tag{18}$$

quantifies the disagreement between the three codes (Table 2, last column). These reference results are commented in Sections 4.1 and 4.2, while the explanations for the observed discrepancies are discussed in Section 5.

[4] For what concerns the plasma domain, "wall" is to be meant as "entire first wall" for SOLEDGE2D and "divertor targets" for SOLPS-ITER and UEDGE.
[5] The rate is actually $2.5 \cdot 10^{21}$ D_2/s in EIRENE.

Region	Quantity ζ	SOLPS-ITER	SOLEDGE2D	UEDGE	Δ
OMP	n_e [m^{-3}] 2.85 cm in core	$6.72 \cdot 10^{20}$	$6.87 \cdot 10^{20}$	$7.67 \cdot 10^{20}$	2-30%
	T_i [keV] 2.85 cm in core	1.57	1.63	1.50	4-8%
	T_e [keV] 2.85 cm in core	1.54	1.60	1.51	2-6%
	SOL n_e decay length [mm]	6.9	6.0	5.2	14-28%
	SOL T_i decay length [mm]	11.5	8.7	14.3	22-49%
	SOL T_e decay length [mm]	6.3	6.2	5.7 (*)	2-10%
Outer target	Peak $q_\parallel$ [MW/m^2]	615	609	695	1-13%
	SOL $q_\parallel$ decay length λ_q [mm]	1.5	1.9	1.2	22-45%
	Peak n_e [m^{-3}]	$7.42 \cdot 10^{21}$	$1.91 \cdot 10^{21}$	$5.85 \cdot 10^{21}$	24-118%
	Peak T_i [eV]	102.6	92.8	112.0	9-19%
	Peak T_e [eV]	49.3	56.0	75.5	13-42%
	T_i [eV] 3.5 cm in PFR	0.46	2.18	0.80	54-130%
	T_e [eV] 3.5 cm in PFR	0.42	1.36	0.66	44-106%
Inner target	Peak $q_\parallel$ [MW/m^2]	266	387	421	8-45%
	Peak n_e [m^{-3}]	$7.00 \cdot 10^{21}$	$5.54 \cdot 10^{21}$	$5.59 \cdot 10^{21}$	1-23%
	Peak T_i [eV]	101.0	103.4	93.0	2-11%
	Peak T_e [eV]	41.2	48.3	71.8	16-54%
	T_i [eV] 3.5 cm in PFR	0.25	1.46	0.79	60-142%
	T_e [eV] 3.5 cm in PFR	0.22	1.13	0.56	67-135%

Table 2: Highlights of the reference results of the three codes with the input parameters of Sections 3.2.1 and 3.2.2. All the scrape-off layer data at the outer mid-plane are considered to compute the density and temperature decay lengths via an exponential fit. In (*), only those points which actually follow an exponential behaviour are employed (Figure 2.c). The power decay length λ_q is instead evaluated by fitting the outer target data remapped at outer mid-plane.

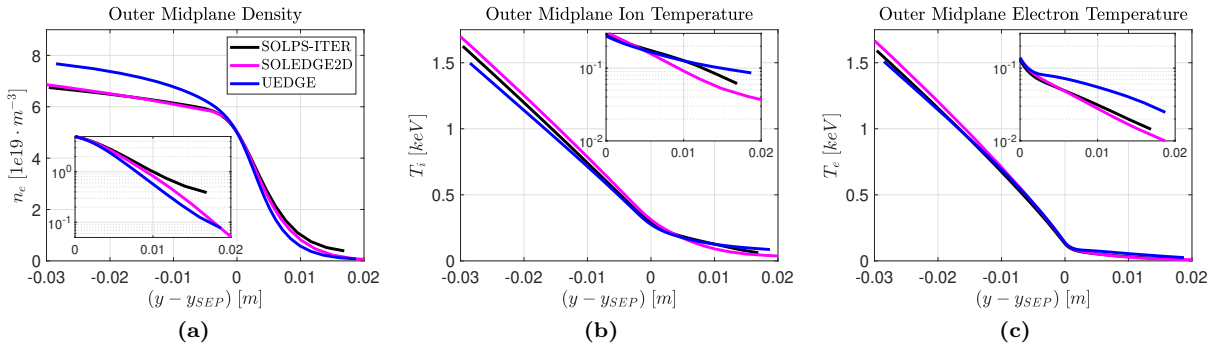

Figure 2: Outer midplane density (a), ion temperature (b) and electron temperature (c) profiles (separatrix at $y - y_{\mathrm{SEP}} = 0$). The insets show, in logarithmic scale, the profiles in the scrape-off layer.

4.1 Outer mid-plane

For the density at OMP (Figure 2), SOLPS-ITER and SOLEDGE2D are in very good agreement, whereas UEDGE predicts a significantly different profile throughout the core, both in terms of shape and of the value attained near the core boundary at $y - y_{\mathrm{SEP}} = -2.85$ cm. The situation is similar for the ion and electron temperature profiles, except the above overestimation of the density by UEDGE corresponds now to an underestimation of the temperatures. It is worthwhile noting that this trend for the density and temperatures is such that the energy density $\varepsilon = nT$ agrees within 11% among the three codes for both ions and electrons in the core.
The overall picture does not change when considering the OMP SOL (insets in Figure 2). The density (ion temperature) decay length among the codes is matched only within 14-28% (22-49%), which results in the far SOL values departing substantially between the three codes. Also, the excellent agreement in the electron temperature decay length in the near-SOL is overshadowed by the UEDGE profile deviating from an exponential decay in the far SOL and remaining significantly higher, such that SOLPS-ITER/SOLEDGE2D values end up being a factor 2 below UEDGE.

4.2 Divertor region

As shown by Figure 3, the comparison of the codes' results at the divertor targets is highly target-specific for the plasma density (and energy densities, not shown): while the peak value attained at the inner target is matched within 1-23%, this discrepancy increases up to 24-118% at the outer target, with SOLEDGE2D departing from the other two codes. At the same time, the peak locations in SOLEDGE2D are found to be ~ 1 cm closer to the strike point than the locations predicted by SOLPS-ITER and UEDGE.
In terms of electron temperature, the leading features of three profiles are similarly scattered. In the SOL at both targets, SOLPS-ITER and SOLEDGE2D show a good agreement in shape and peak value, except that the SOLEDGE2D profile has the onset of the temperature increase occuring 1.7 cm closer to the strike point than for SOLPS-ITER and UEDGE. However, UEDGE peak electron temperature (and overall profile) lies up to 54% above SOLPS-ITER's. This feature may be connected to the similar T_e discrepancy observed for UEDGE upstream in the OMP far-SOL. The ion temperature qualitatively behaves in a similar manner, but featuring a much better quantitative agreement in the SOL between UEDGE and the other codes. Instead, in the outer and inner target PFR, T_i departs up to a factor 4 and 5, respectively, with the extremes embodied by SOLPS-ITER (below) and SOLEDGE2D (above), UEDGE sitting in between.
Despite the 22-45% disagreement among the codes, $\lambda_q < 2$ mm remains in line with its predicted value [4][5]. The parallel heat flux at the outer target is remarkably well matched by the three codes, disagreeing by 1-13%, while the SOLPS-ITER peak lies below the one of the other two codes at inner target, resulting in a disagreement of 8-45%. An analogous picture holds for its perpendicular counterpart $q_\perp = q_\parallel \cdot \sin\vartheta$ that, with the grazing angle $\vartheta \sim 0.025$ rad for both targets, attains a maximum of 7-10.5 MW/m^2 and of

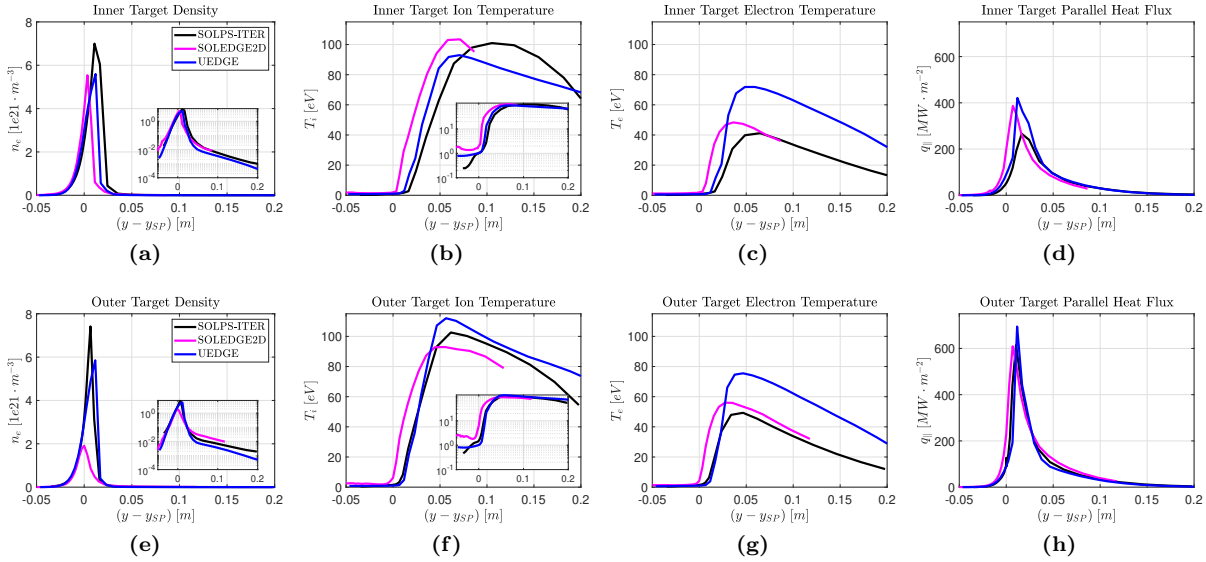

Figure 3: Inner (from a to d) and outer (from e to h) target profiles (strike point at $y - y_{\mathrm{SP}} = 0$) for SOLPS-ITER, SOLEDGE2D and UEDGE, showing plasma density, ion temperature, electron temperature and parallel heat flux, from left to right. The insets show the density and ion temperature profiles in logarithmic scale.

16-17.8 MW/m^2 at inner and outer target, respectively.
The integrated radiation sink, with a dominance of line radiation over Bremsstrahlung emission and hence concentrated in the divertor volume, accounts for 0.61 MW, 0.52 MW and 0.64 MW ($\leq 8\%$ of P_{SOL}) for SOLPS-ITER, SOLEDGE2D and UEDGE, respectively, thus varying of 4-21% among the codes.
The neutral density distributions (n_{g}, Section 2.2) in Figure 4 differ in the PFR between the three codes. SOLPS-ITER (SOLEDGE2D) displays an inner-outer-target asymmetry of a factor ~ 3 in the distribution, with n_{g} peaking at $4.07 \cdot 10^{21}$ m^{-3} ($1.59 \cdot 10^{21}$ m^{-3}) around the inner strike point, at $1.54 \cdot 10^{21}$ m^{-3} ($0.49 \cdot 10^{21}$ m^{-3}) around the outer. Similarly for the neutral pressure p_{g}, which reaches 32.8 Pa (7.2 Pa) and 12.7 Pa (3.7 Pa) at the inner and outer pump entrance (see Figure 1 for locations). The opposite is true for the more symmetric UEDGE neutral density, peaking at $3.52 \cdot 10^{21}$ m^{-3} and $3.07 \cdot 10^{21}$ m^{-3} around the inner and outer strike point, respectively. Also, in the region below the X point the UEDGE density is larger than SOLPS-ITER's (SOLEDGE2D's) by a factor 3 (4). Finally, it's worth noting that the SOLPS-ITER plasma PFR boundary is clearly visible in the neutral density plot, showing an abrupt change in n_{g} across the boundary location, indicating this artificial numerical feature may have impact on the code results.

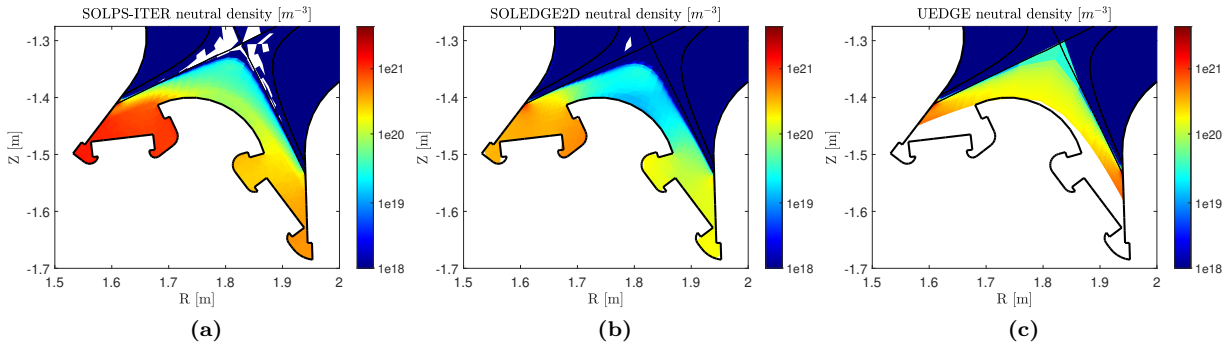

Figure 4: Divertor neutral density ($n_{\mathrm{D}} + 2n_{\mathrm{D}_2}$) maps for SOLPS-ITER ($a$) and SOLEDGE2D ($b$). Blank cells result from the absence of any neutral particle being able to reach them. Atom density (n_{D}) map for UEDGE (c). In-plasma black lines are the SOLPS-ITER separatrix and the scrape-off layer $1\lambda_q$ away from the separatrix.

5 Discussion

In the following sections, first, the importance of the differences intrinsic to the three plasma models are quantitatively estimated. Then, the validity of the UEDGE $T_g = T_i$ simplification adopted in the fluid neutral model is discussed with respect to the kinetic model of SOLPS-ITER and SOLEDGE2D. Last, on the basis of the previously-established knowledge, the differences in the results presented in Section 4 are thoroughly investigated.

5.1 Intrinsic differences in plasma equations

Outlined in Section 2.1, the SOLPS-ITER plasma equations include additional terms absent in the other two codes. In this section, the relative impact of these terms on the plasma solution will be quantitatively assessed, and conclusions drawn.

For SOLPS-ITER x-directed advective fluxes[6], $V^{\text{diff}}_{\text{i}x,n}$ (rescaled by a factor 5/3 in the energy equations) and $V^{\text{corr}}_{\text{i}x}$ are added to the plasma fluid speed $b_x V_{\text{i}\parallel}$. Their relative weight $\left|V^{\text{diff}}_{\text{i}x,n}\right| / (\left|b_x V_{\text{i}\parallel}\right| + \left|V^{\text{diff}}_{\text{i}x,n}\right| + |V^{\text{corr}}_{\text{i}x}|)$ and $|V^{\text{corr}}_{\text{i}x}| / (\left|b_x V_{\text{i}\parallel}\right| + \left|V^{\text{diff}}_{\text{i}x,n}\right| + |V^{\text{corr}}_{\text{i}x}|)$ throughout the plasma domain is on average 1.2% and 0.8%, although attaining, respectively, a maximum of 26% and 80% around the X point where $b_x V_{\text{i}\parallel} \to 0$.

Furthermore, SOLPS-ITER includes the anomalous transport (Section 2.2.1) along the poloidal direction x, e.g. $\left(\kappa^{\text{CL}}_{\text{e}x} + \kappa^{\text{AN}}_{\text{e}}\right) \partial_x T_{\text{e}}$ in SOLPS-ITER vs. $\kappa^{\text{CL}}_{\text{e}x} \partial_x T_{\text{e}}$ in SOLEDGE2D and UEDGE (similar expressions hold for the ion heat and viscous transport). The relative importance of the anomalous-coefficient-dependent term with respect to the overall corresponding poloidal flux is the primary judgement metric. The resulting pictures of $|\kappa^{\text{AN}}_{\text{ei}} \partial_x T_{\text{ei}}|$ for the electron and ion heat transport and $|\eta^{\text{AN}}_{\text{i}} \partial_x V_{i\parallel}|$ for the viscous transport are shown in Figure 5. The anomalous transport contribution to the overall flux along x is mainly noticeable in the PFR, where the classical coefficient ($\propto T^{5/2}$ [35]) becomes vanishingly small as there is virtually no plasma, and thus is of little concern in this region. Independently of the classical coefficient being flux-limited or not, the effect on the electron (ion) heat transport ranges from 25% to 40% (from 35% to 60%) in the vicinity of the strike points, while being negligible elsewhere in the near-separatrix SOL (delimited by the separatrix and the adjacent, $1\lambda_q$ away, black line in Figure 5), a region of particular relevance. Since the proximity of the strike point is only scarcely populated by the plasma, which features a temperature < 5 eV characteristic of detachment, the possible impact of the anomalous terms further decreases. The anomalous viscosity instead accounts on average for 13% throughout the divertor near-separatrix SOL, attaining a maximum value of 87% around the X point and 67% at the inner target.

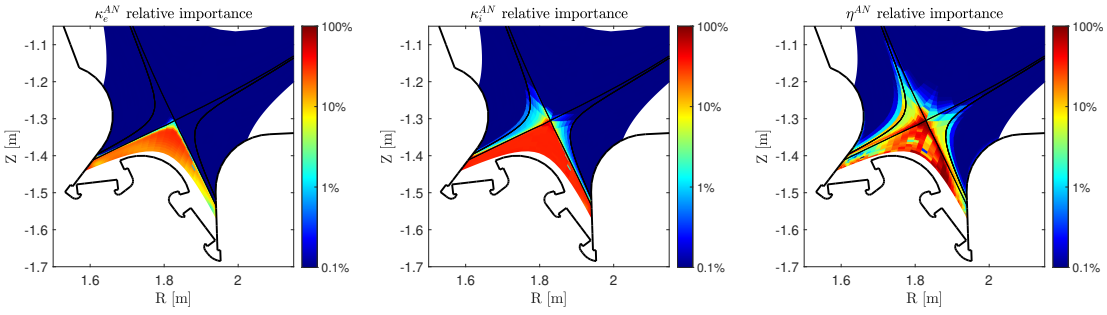

Figure 5: Relative importance (see text) of the term depending on the anomalous electron heat (a), ion heat (b) and viscous (c) transport coefficient along x in SOLPS-ITER equations. This contribution is absent in SOLEDGE2D and UEDGE.

Last, SOLPS-ITER geometry-related terms can have an effect on the far SOL and core (9%, on average), but practically vanish ($\ll 1\%$) in the near-separatrix SOL.

At the time of writing there is no clear evidence pointing to a completely negligible impact of the terms

[6] $\mathbf{V}_{\text{e}} = \mathbf{V}_{\text{i}}$ in absence of drifts and currents (Section 2.1).

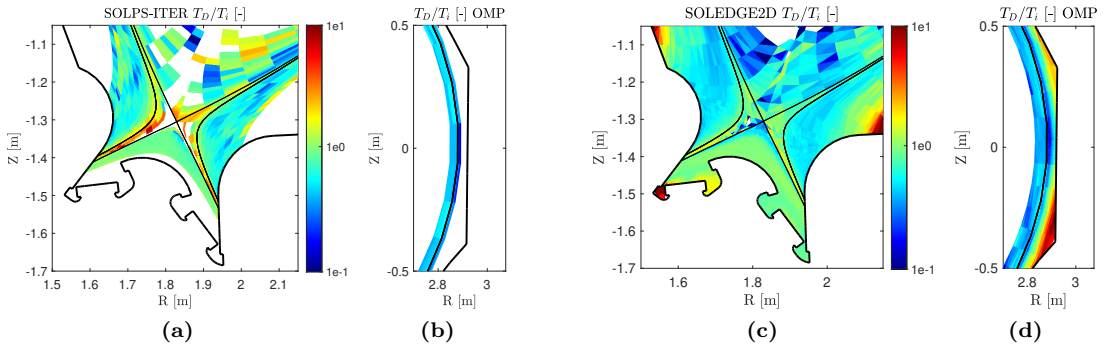

Figure 6: SOLPS-ITER (a and b) and SOLEDGE2D (c and d) atoms-to-ions temperature ratio throughout the plasma. Zooms at outer-midplane are also shown. The statistical fluctuation of the values is due to the finite number of Monte Carlo histories employed by EIRENE.

discussed above on the final results. Though the fact that the SOLPS-ITER results do not show significant deviation from the general trends set by SOLEDGE2D and/or UEDGE in regions where such terms take quantitative significance suggests that their impact is minimal under the chosen scenario.

5.2 Suitability of UEDGE ion-neutral shared temperature assumption

Section 2.2 introduced the different approaches followed by SOLPS-ITER, SOLEDGE2D and UEDGE to model neutral particles. In this paragraph, the justifiability of the UEDGE $T_g/T_i = 1$ is discussed.
The hypothesis of a common ion-neutral temperature is supported by the quick thermal equilibration via atomic CX (Section 2.2), which is, according to SOLPS-ITER output data, the dominant reaction along with molecular CX and EL, accounting for 52%, on average, in the plasma and in the near-separatrix SOL, and up to 56% in the PFR with respect to all the 11 reactivity-related reactions (Section 2.2).
By computing the atoms-to-ions temperature ratio T_D/T_i throughout the plasma domain (Figure 6), the UEDGE assumption $T_g/T_i = 1$ appears reasonable in certain regions. If T_D/T_i is weighted in each mesh cell by the number of D atoms in that cell normalised to the total number of atoms in the simulation, the computed weighted average value reads 1.02 and 1.11 in the whole plasma domain for SOLPS-ITER and SOLEDGE2D respectively, and in SOLPS-ITER it lies around 1.01 in the divertor volume where the presence of neutrals is particularly significant. Apart from some scattered cells badly affected by MC noise, the only region in the divertor where $T_g/T_i = 1$ is violated by some margin (i.e. $T_D/T_i \sim 10$, at most) sits in the near-separatrix SOL for SOLPS-ITER. This feature is instead absent in SOLEDGE2D[7] ($T_D/T_i \sim 1.8$ at most). Indeed, only few ($n_D/n_i \ll 1\%$) highly energetic SOLPS-ITER neutral atoms are able to reach this region, due to the high plasma density and flux (Figure 3) and atom-plasma reactions localised in the near-separatrix SOL, but still result in $T_D/T_i > 1$. Therefore, given the scarce neutral population living in this divertor subregion, the $T_g/T_i \sim 1$ violation is of little concern.
Instead, for the OMP in the upstream main chamber, T_D/T_i (T_g/T_i) drops to 0.15 (0.07) (Figure 6.b and .d) for both SOLPS-ITER and SOLEDGE2D. This feature and its implications for the UEDGE model are discussed in Sections 5.3 and 5.4.

5.3 Differences in OMP core

As clearly seen in Figure 2, profiles for the plasma density and electron and ion temperature show significant disagreement in the OMP core, with UEDGE profiles departing from those of SOLPS-ITER and SOLEDGE2D. In particular, the higher core density and steeper density gradients in UEDGE imply an enhanced volumetric particle ionization source within the separatrix, a likely cause being an increased neutral penetration in UEDGE with respect to the other two codes. This subsection investigates the

[7]The near-wall regions outside SOLPS-ITER/UEDGE SOL artificial boundary are such that $T_D/T_i > 1.25$ in SOLEDGE2D. This is due to the <10-eV ion, >10-eV atom temperature in these limiter-like portions of space and is not of any concern.

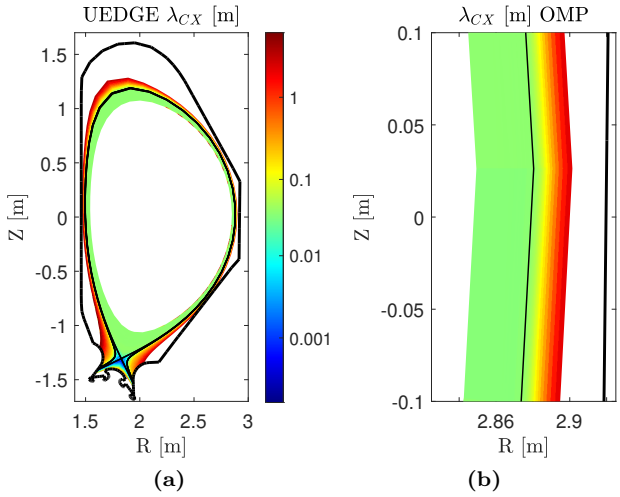

Figure 7: Charge exchange mean free path $\lambda_{\rm CX} = \sqrt{T_{\rm i}/m_{\rm i}}/(n_{\rm i}\langle\sigma v\rangle_{\rm CX})$ for neutral D atoms throughout the UEDGE domain (a) in the reference case settings. The zoom at outer-midplane is also shown (b).

settings adopted (either explicitly, implicitly or by default) for the neutrals, a fact of special relevance at the OMP given the vicinity to the puffing port from which neutral particlefs are injected in the domain (Figure 1).
First, the condition $T_{\rm g} = T_{\rm i}$ throughout the domain (Sections 2.2 and 5.2) links the neutral CX mean free path $\lambda_{\rm CX}$ to the local ion temperature. This is of particular importance for UEDGE at the boundary: the temperature at which puffed or recycled atoms are injected is therefore implicitly fixed at the ion's. Conversely, the puffing temperature $T_{\rm puff}$ can be user-selected in EIRENE where its default value is 0.03 eV, i.e. room temperature. Specifically, with the reference results of Section 4.1, the temperature computed by UEDGE in the outermost OMP cell where the gas puffing is located is $\sim$ 83 eV. This high and unrealistic neutral temperature results in a CX mean free path $\lambda_{\rm CX} = \sqrt{T_{\rm i}/m_{\rm i}}/(n_{\rm i}\langle\sigma v\rangle_{\rm CX}) \sim 2$ m at the OMP boundary – much longer than the OMP domain width, providing strong potential for neutrals to penetrate into the core region. Indeed, calculating the integrated neutral flux crossing the separatrix into the core region, fluxes are found to be the equivalent of $2.23 \cdot 10^{21}$ D/s in SOLPS-ITER (combined atom and molecule fluxes), and $3.30 \cdot 10^{21}$ D/s for UEDGE, $\sim$ 50% higher. Figure 7 shows that this long $\lambda_{\rm CX}$ issue is not limited to just the OMP, but concerns the entire SOL domain edge boundary, at least outside the near-separatrix SOL.

The impact of the $T_{\rm g} = T_{\rm i}$ assumption can be assessed by: (i) reducing the neutral temperature in the whole UEDGE plasma domain, setting $T_{\rm g} = c\, T_{\rm i}$ with c = 25%, 15% and 10% to mimic a decrease of $T_{\rm puff}$ towards 0.03 eV; (ii) adjusting the neutral flux limit factor $\alpha_{\rm g}$ from 1.00 (default, Section 2.2.1) to 0.50, 0.32 and 0.25 in UEDGE, thus limiting the magnitude of neutral transport and therefore the neutral penetration depth, regardless of $T_{\rm g}$; (iii) setting $T_{\rm puff}$ in EIRENE to the same value computed by UEDGE in the outermost OMP cell (83 eV). This last choice leads SOLPS-ITER to a final $T_{\rm g}$ ($T_{\rm i}$) rising from 1 eV (61 eV) to 36 eV (120 eV) in the outermost OMP cell: despite the substantial improvement toward the UEDGE value, a non-negligible difference still exists.
In the following, SOLPS-ITER data are implicitly referred to, although the same qualitative reasoning holds for SOLEDGE2D and UEDGE as well. The results of investigations for (i) are shown in Figure 8. As $T_{\rm g}$ is decreased, the differences between the UEDGE and SOLPS-ITER profiles is reduced. At $c = 15\%$ (notably the equivalent ratio as the average $T_{\rm D}/T_{\rm i}$ obtained for the SOLPS-ITER/SOLEDGE2D OMPs – Section 5.2), the difference between the core profiles is almost entirely removed. This corresponds with a reduction of $T_{\rm g}$ to 6.9 eV, and a shorter CX mean free path, reducing the neutral penetration across the separatrix to $2.21 \cdot 10^{21}$ D/s (now in line with the SOLPS-ITER value of $2.23 \cdot 10^{21}$ D/s). However, further reducing c to 10% causes an over-correction to the UEDGE profiles, with a core density profile

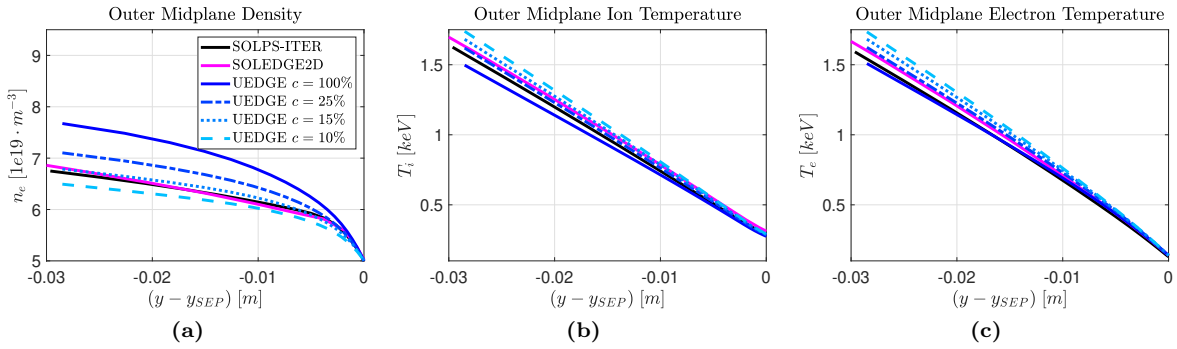

Figure 8: Scan of UEDGE neutral-to-ion temperature ratio $c = T_g/T_i$ from 100% (default, $\sim$ high T_{puff}) to 25%, 15% and 10% ($\sim$ low T_{puff}), showing outer mid-plane density (a), ion temperature (b) and electron temperature (c) core profiles.

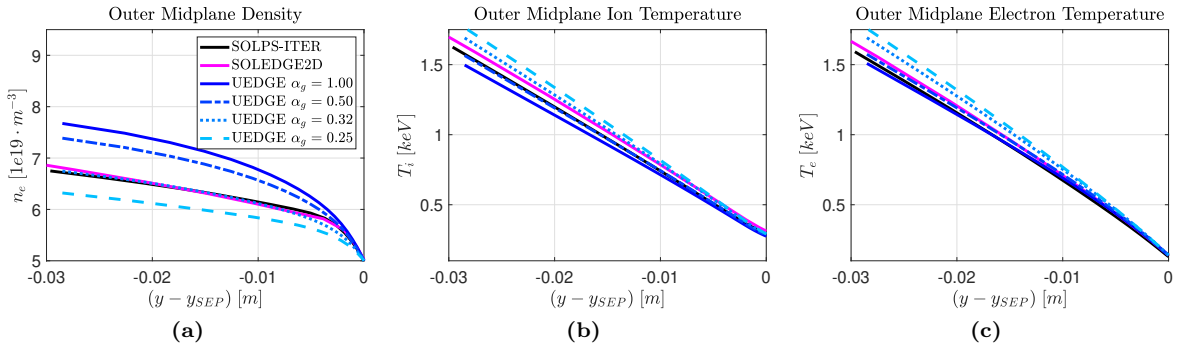

Figure 9: Scan of UEDGE neutral flux limiter α_g from 1.00 (default, $\sim$ high penetration) to 0.50, 0.32 and 0.25 ($\sim$ low penetration), showing outer mid-plane density (a), ion temperature (b) and electron temperature (c) core profiles.

becoming too low and temperatures too high in relation to the SOLPS-ITER profile.
Similarly, results of (ii) show the same effect for reduction of the neutral flux limiters (Figure 9): lowering the magnitude of the flux-limit factor reduces and eventually eliminates (with $\alpha_g = 0.32$) the differences in the core profiles between the codes. Again, an over-correction is observed when α_g is reduced further to 0.25. However, changing these flux limiters implies aprioristically assuming a maximum scale for neutral diffusivity, which is a physically dubious assumption – the "correct" flux limiter required to match the MC simulations is likely dependent on the local plasma conditions, SOL geometry, etc. That a reduction of either the UEDGE neutral temperature or the flux-limit factors is able to correct for the OMP differences observed gives a strong indication that indeed the enhanced neutral penetration in UEDGE is the cause of the discrepancies.
Results of (iii) are shown in Figure 10. For increasing T_{puff}, there is undoubtedly a strong positive correlation between the puffed neutral temperature and the plasma density in the core, with the core densities of SOLPS-ITER and SOLEDGE2D eventually matching that of UEDGE. Indeed, the CX rate at OMP, a source of energetic neutrals which helps their penetration, grows by a factor ~ 1.2 for atomic CX and by more than an order of magnitude for molecular CX (present in SOLPS-ITER only) in the core and the near-separatrix SOL, as depicted in Figure 11. This leads to a 2-fold increase of the neutral flux through the separatrix (dominated by the 38-fold increase for molecules) and ultimately to an increase of neutral EI and DS (volumetric particle sources in Eq. 1) of a factor 5-10 in the core. This forces the density core profile to inflate and depart from its initial SOLPS-ITER/SOLEDGE2D-like linear shape ($\sim$ pure diffusion along y, Section 2.2.1) in the direction of the non-linear UEDGE-like profile ($\sim$ diffusion along y with volumetric sources).

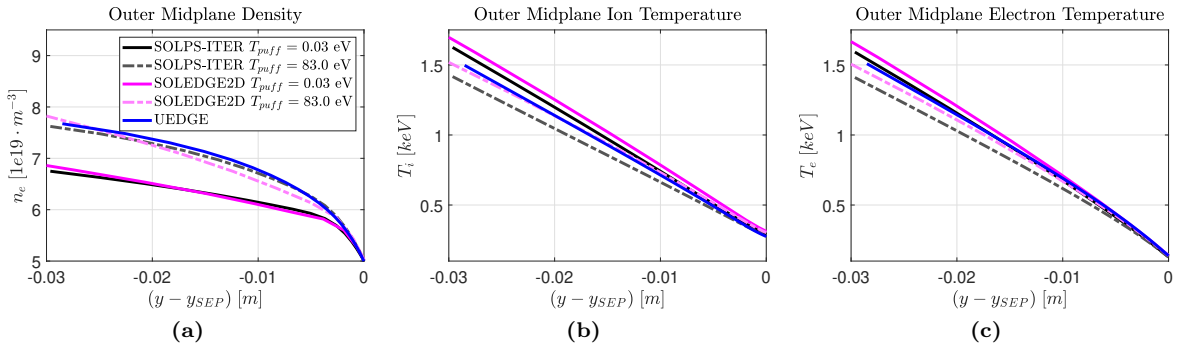

Figure 10: Scan of SOLPS-ITER and SOLEDGE2D puffed neutral temperature T_{puff} from 0.03 eV (default) to 83 eV, showing outer mid-plane density (a), ion temperature (b) and electron temperature (c) core profiles.

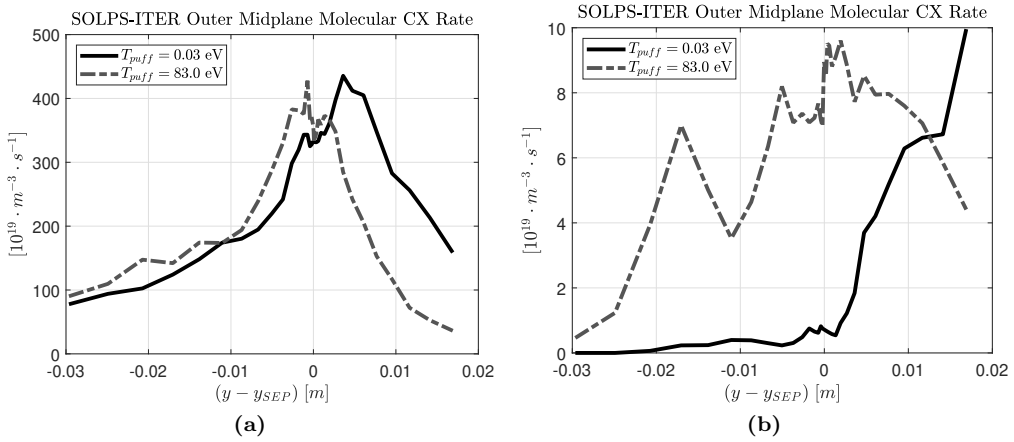

Figure 11: SOLPS-ITER outer mid-plane atomic (a) and molecular (b) CX reaction rate per unit volume for a puffed neutral temperature of $T_{\text{puff}} = 0.03$ eV (default) and 83 eV.

The minor 5% disagreement between SOLPS-ITER and SOLEDGE2D with $T_{\text{puff}} = 0.03$ eV is robustly retained when T_{puff} grows to 83 eV despite SOLEDGE2D not including molecular CX. This is presumably due to a compensation by the more dominant atomic CX (a factor 40 above for SOLPS-ITER), coming into play as soon as molecules undergo EI or DS in the SOL.
Therefore, despite the validity of the UEDGE assumption $T_{\text{g}} = T_{\text{i}}$ in the divertor region (Section 5.2), this analysis leans towards the need for the development in the UEDGE fluid-neutral model of an individual neutral energy equation that solves for T_{g} separately. Such a condition has been implemented in a very recent version of UEDGE [25], but was not publicly available at the time of these studies. However, whether this change would fully resolve the observed issues is currently unclear, which may be more fundamentally connected to the fluid-vs-kinetic treatment of the neutral species.
The above discussion helps in explaining the differences in the ion temperature profiles as well. Indeed, CX being an ion-neutral temperature-equilibrating mechanism (Section 2.2), the increased cold neutral flux crossing the separatrix with $T_{\text{puff}} = 83$ eV naturally leads to a 13% decrease of both the SOLPS-ITER and SOLEDGE2D core ion temperature toward UEDGE's. The ion-electron temperature equilibration then implies a very similar decrease (11%) of the core electron temperature, coherent with an overall core plasma cooling due to the more penetrating neutrals.

5.4 Differences in OMP SOL and at targets

The previous core-related discussion leads the expectation that differences in the OMP SOL quantities be directly related to those observed for the core. As such, the SOL plasma density profile for UEDGE approaches those of SOLPS-ITER and SOLEDGE2D for the changes in neutral temperature factors c and neutral flux limiters α_{g}, as before (Figures 12 and 13 for the SOL similar to Figures 8 and 9 for the core). The same approach varying T_{puff} does not yield analogous results for SOLPS-ITER and SOLEDGE2D: the partial correspondence with neutrals behavior in UEDGE is completely lost due to the kinetic treatment in addition to the unrealistic $T_{\text{g}} \sim 83$ eV in the far SOL.

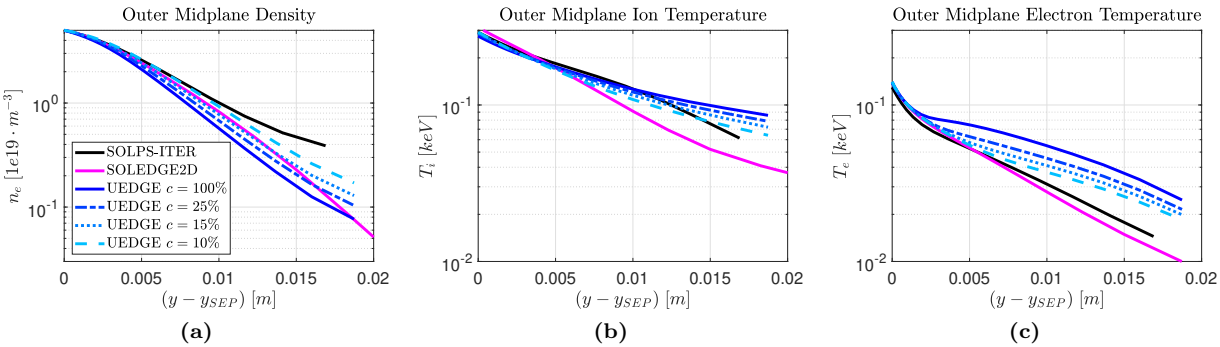

Figure 12: Scan of UEDGE neutral-to-ion temperature ratio $c = T_{\text{g}}/T_{\text{i}}$ form 100% (default) to 25%, 15% and 10%, showing outer mid-plane density (a), ion temperature (b) and electron temperature (c) scrape-off-layer profiles.

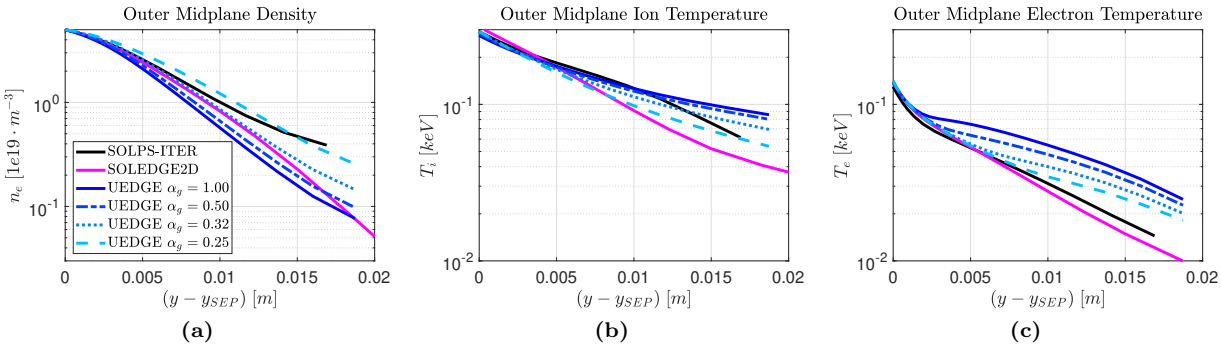

Figure 13: Scan of UEDGE neutral flux limiter α_g from 1.00 to 0.50, 0.32 and 0.25, showing outer mid-plane density (a), ion temperature (b) and electron temperature (c) scrape-off-layer profiles.

This SOL effect has a clear physical motivation, beyond the consistency with the core behavior. For decreasing c, the weaker penetration of the puffed neutrals results in EI and DS peaking less deeply into the plasma, therefore in higher peripheral sources and plasma density. As a consequence, the outward-projected anomalous radial flux from the core $-D^{\mathrm{AN}}\partial_y n_{\mathrm{i}}$ (Section 2.2.1) weakens, ultimately leading to a larger SOL density decay length. Correspondingly, the UEDGE ion and electron SOL temperature profiles tend to agree with SOLPS-ITER/SOLEDGE2D as c decreases and the UEDGE SOL density profile increases, indicating that the neutral penetration issue is also the causal factor for this observed discrepancy.

Comparing the far SOL ($y - y_{\mathrm{SEP}} \geq 0.015$ m) density profiles, the SOLEDGE2D profile lies below those of SOLPS-ITER and the adjusted UEDGE cases. This may result from the different plasma mesh extensions in these latter codes, i.e. the impact of the artificial plasma BCs and/or neutral recycling source at the domain edge.

The discrepancy in the electron and ion temperatures between the UEDGE results and those obtained with the other codes could be ascribed to a smaller ion-electron thermal coupling ($K_{\mathrm{EQ}}(T_{\mathrm{e}} - T_{\mathrm{i}}) \propto n_{\mathrm{i}}^2(T_{\mathrm{e}} - T_{\mathrm{i}})/T_{\mathrm{e}}^{3/2}$ in Eq. 15) caused by the lower ion density in UEDGE by a factor 1.5-4 with respect to the other codes (Figures 12.a and 13.a) [44].

The discrepancies observed for UEDGE in the upstream far-SOL are also present at the target plates: the density is lower with respect to SOLPS-ITER and SOLEDGE2D, and the electron temperatures are higher. Given the strong connection between the upstream and divertor quantities in the attached sheath-limited regime [19], it could be postulated that the solutions applied to reduce the UEDGE discrepancies at the OMP may also improve the agreement at the target plates. In particular, the flux limiter solution may be the most appropriate, given that $c = T_{\mathrm{g}}/T_{\mathrm{i}} \sim 1$ is a reasonable assumption in the divertor region (Section 5.2).

Figure 14 shows the evolution of the divertor profiles for reduced UEDGE neutral flux limiter. Whilst the far-SOL electron temperature decreases and the plasma density changes appropriately, demonstrating the connection between these discrepancies to those upstream, the agreement with the other codes has not improved in general, and the UEDGE ion temperature disagreement significantly worsens. This shows that reducing α_{g} may not be a good overall solution to the issues observed for UEDGE: well-separated scales of neutral diffusion exist in the OMP and in the divertor SOL, so that any attempt at artificially fixing the differences via α_{g} may lead to improvements in one region but simultaneously to detrimental consequences elsewhere.

5.5 Differences in PFR at targets

This section deals with the differences in the EIRENE reactions as implemented by SOLPS-ITER and SOLEDGE2D (Table 1). SOLEDGE2D does not include any ion-molecule temperature-equilibrating mechanisms, i.e. molecular CX and EL. Moreover, apart from those in common with SOLPS-ITER, SOLEDGE2D employs one-parameter (ion temperature) fits (1Pfit) to compute the remaining reactivities, whereas SOLPS-ITER uses their two-parameter [ion temperature and (neutral temperature or ion

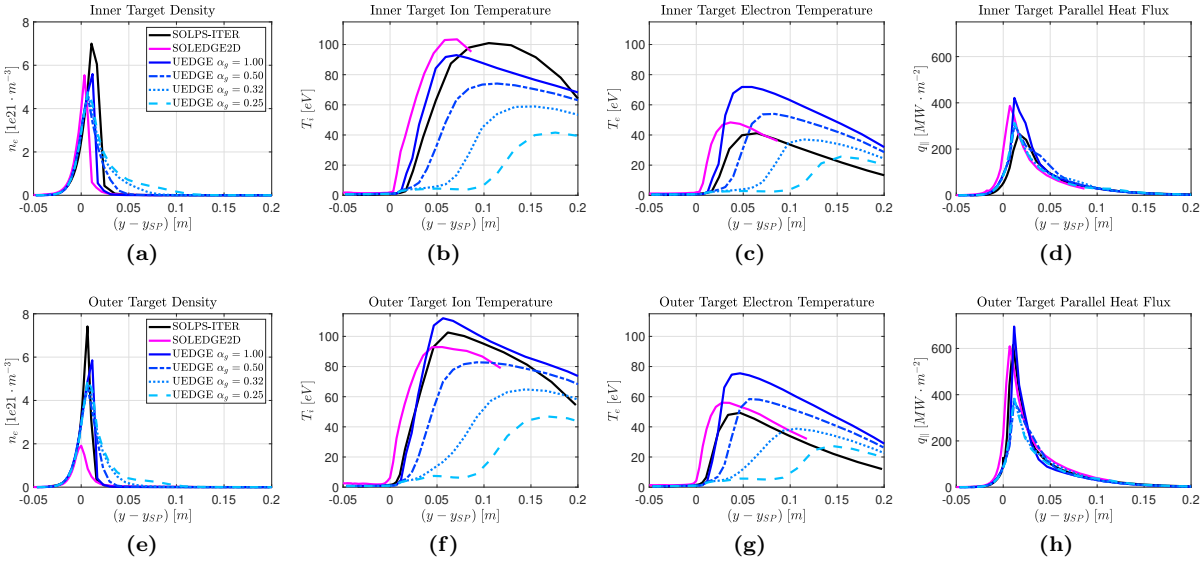

Figure 14: Scan of UEDGE neutral flux limiter α_g from 1.00 to 0.50, 0.32 and 0.25 , showing inner (a to d) and outer (e to h) target profiles, showing density (miniature in logarithmic scale), ion and electron temperature, and parallel heat flux profiles from left to right.

density)] counterparts (2Pfit). The importance of these differences can be quantified as follows.
First, reactions are grouped on the basis of the EIRENE reactant involved (similarly to Eq. 10). Then, by employing one- (SOLEDGE2D-like) and two-parameter (SOLPS-ITER-like) fits, $(S_{\mathrm{i,D}})_{1\mathrm{Pfit}}$ and $(S_{\mathrm{i,D}})_{2\mathrm{Pfit}}$ (and analogously for D_2 and D_2^+) are obtained, respectively. Only the SOLPS-ITER computed densities and temperatures are used in evaluating these terms so that the differences, if any, will retain only information about the reactivity fits themselves. This approach also allows a 2D representation in the plasma domain and to weight the differences by the importance of the r^{th} reaction with respect to all the others involving the same reactant. The ratios $(S_{\mathrm{i,D}})_{1\mathrm{Pfit}}/(S_{\mathrm{i,D}})_{2\mathrm{Pfit}}$, $(S_{\mathrm{i,D_2}})_{1\mathrm{Pfit}}/(S_{\mathrm{i,D_2}})_{2\mathrm{Pfit}}$ and $(S_{\mathrm{i,D_2^+}})_{1\mathrm{Pfit}}/(S_{\mathrm{i,D_2^+}})_{2\mathrm{Pfit}}$ are pictured in Figure 15.
Regarding the atomic (molecular ion) reaction rates, SOLEDGE2D 1Pfit differ by only 6% (8%) from the SOLPS-ITER 2Pfit, on average. Still, the disagreement of atomic CX increases up to 18% in the near-separatrix divertor SOL, and further up to 47% near the outer strike point. This is not considered a significant issue *per se*, given the negligible neutral density in this volume ($n_g/n_i \ll 1\%$). Molecular reactions feature an average substantial disagreement of 46%, to which the missing molecular CX and EL

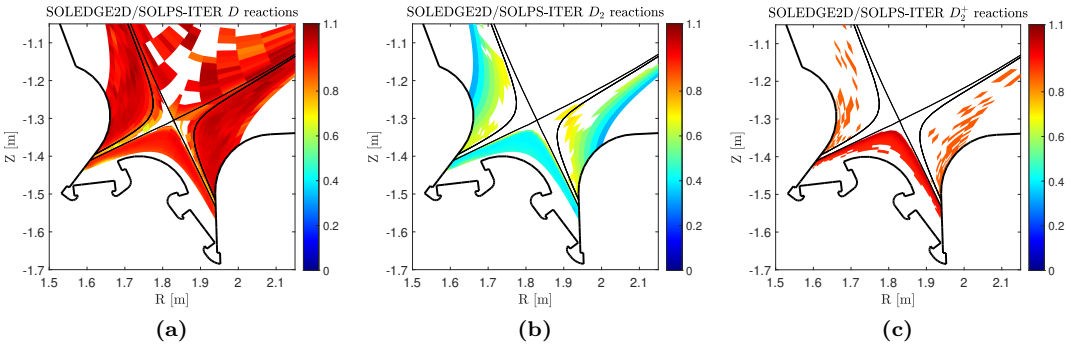

Figure 15: Cell-by-cell ratio between SOLEDGE2D and SOLPS-ITER reaction rates involving atoms (a), molecules (b) and molecular ions (c) as computed via the respective fits for the reactivities (Table 1). Density and temperature data employed are those of SOLPS-ITER.

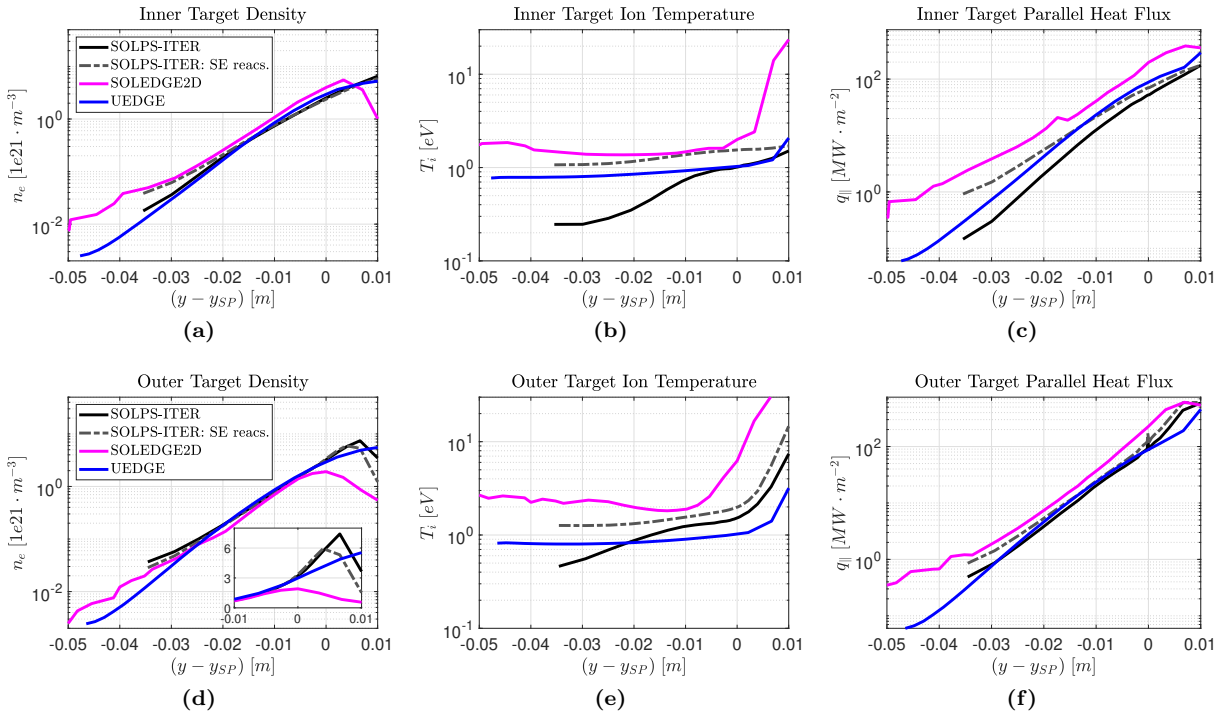

Figure 16: SOLPS-ITER, SOLPS-ITER with SOLEDGE2D reactions (SE reacs.), SOLEDGE2D and UEDGE inner (a to c) and outer (d to f) target density, ion temperature and parallel heat flux, from left to right. The abscissa is chosen to mainly emphasize the private-flux region. The miniature in the outer target density shows the profile with a linear scale and zoomed-in abscissae.

are to be added. Therefore, SOLPS-ITER has been run with the SOLEDGE2D set of reactions (Table 1).

In the matter of the *integral* power radiated, SOLPS-ITER figure increases from 0.61 MW (Section 4.2) to 0.67 MW, hence further departing from the 0.52 MW obtained by SOLEDGE2D.

Locally, the OMP profiles (not shown) are not significantly affected (2% variation at most). In both OMP core and SOL, this is presumably due to atomic CX that, in spite of some disagreement (5% at most, 2% on average at OMP), dominates over the other reactions, especially with $T_{\text{puff}} = 0.03$ eV (Figure 11). The newly obtained profiles at the targets are shown in Figure 16. Generally speaking, the change in the reactions affects the inner target (undergoing modifications by a factor 2-6) more than the outer one (factor 1.3-2). Irrespective of this, the SOLPS-ITER profiles[8] always more closely approach those of SOLEDGE2D.

The decrease of 40% in the peak density value improves the similarity to the SOLEDGE2D profile in the PFR (21% closer) and moves the outer target peak density towards SOLEDGE2D's, although remaining substantially above. This is the only paramemter non-negligibly influenced in the SOL by the change in the reactions, possibly because of the drop of 47% in the atomic CX when moving to a 1Pfit (Figure 15.a) which would lead to a defect of plasma sources (EI) and thus density, where neutrals are impeded in penetration (i.e. near-strike-point SOL).

The inner and outer target ion temperatures increase in the PFR towards SOLEDGE2D's to within a factor of 1.4-1.5, confirming both the importance of reactions in the PFR itself and, indirectly, the appropriateness (within a factor 1.4-1.5) of the artificial PFR boundary condition employed by SOLPS-ITER (similarly for the density). Indeed, due to the ion-neutral thermal decoupling obtained by excluding molecular CX and EL (Section 5.3), the ratio $T_{\text{D}_2}/T_{\text{i}}$ ($T_{\text{g}}/T_{\text{i}}$) coherently drops in the PFR from 0.62 (0.72)

[8]The SOLPS-ITER heat flux spikes at the strike point $(y - y_{\text{SP}}) = 0$, also appearing in [40] and being discussed in [43], are not of concern. Instead, the SOLEDGE2D profiles not smoothly developing in the far PFR are probably due to the mesh-wall orthogonality not being satisfied anymore [45].

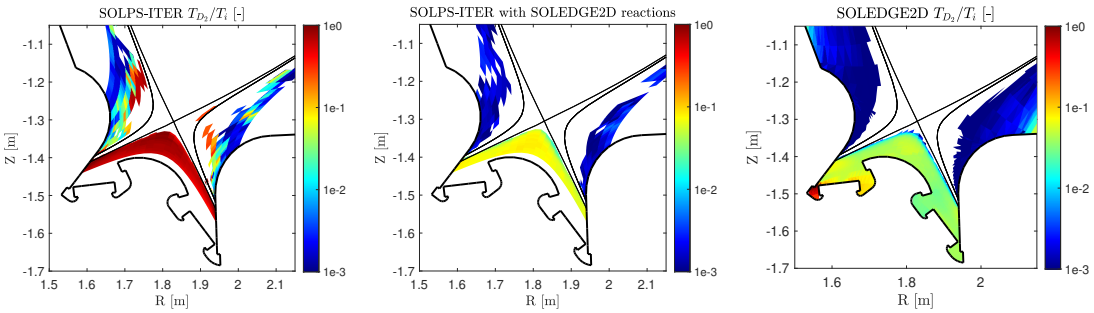

Figure 17: SOLPS-ITER (a), SOLPS-ITER with SOLEDGE2D reactions (b) and SOLEDGE2D (c) molecules-to-ions $T_{\mathrm{D}_2}/T_{\mathrm{i}}$ temperature ratio in the divertor region.

to 0.07 (0.36) − weighted averages as in Section 5.2, giving the opportunity to the ion temperature to rise approaching SOLEDGE2D's[9] (Figure 17). Removing the ion-neutral temperature-equilibrating mechanisms could also explain: (i) the lower agreement with UEDGE at the outer target (see Section 5.6 for inner target), for which $T_{\mathrm{g}} = T_{\mathrm{i}}$; (ii) the influence of higher neutral density at the inner PFR boundary (Figure 4) on recovering the initial (that is, including molecular CX and EL) 0.25 eV ion temperature in that region, a factor 2 closer than its outer counterpart to the wall temperature of 0.1 eV (Section 3.2.2), with which the molecules thermalise.
Moreover, when employing SOLEDGE2D one-parameter fits, the minimum recommended temperature spans the range 0.1-3.98 eV [30], while SOLPS-ITER two-parameter fits allow a less constraining lower bound (0.05-0.1 eV [29]). In the present case, the SOLEDGE2D minimum ion temperature ~ 1 eV violates by a small margin the 3.98 eV limit. On the other hand, SOLPS-ITER ion temperatures with CX and EL included suggest that a minimum temperature lower than 1 eV would appear more reasonable (Figure 16.b and .e). This value, substantially violating the aforementioned limit, would lead to overestimations up to 10^3-10^5 in the PFR. In different scenarios (e.g. higher degree of divertor openness, lower temperatures, and important presence of molecules, as in a detached regime) this effect may be exacerbated.
Concluding this section, it appears that including molecular CX and EL and switching to two-parameter fits in SOLEDGE2D would surely be worthwhile. A valuable improvement would also come from keeping under control the range of validity of the reactivities when running SOLEDGE2D and, in the near future, the upgraded SOLPS-ITER with an extended plasma mesh [46] reaching low-temperature low-density regions.

5.6 Differences in PFR

In this section, differences in the neutral PFR distributions of Figure 4 are discussed in the light of the central role played by the reactions in this region.
The SOLPS-ITER and SOLEDGE2D results mainly differ in terms of gradients determining the abrupt change in n_{g} across the SOLPS-ITER PFR boundary location. Figure 18 shows, from left to right, the molecular density obtained by SOLPS-ITER with its own default set of reactions, by SOLPS-ITER with SOLEDGE2D set of reactions (Section 5.5), and by SOLEDGE2D.
Changing the SOLPS-ITER reaction set greatly reduces the observed discrepancy between the codes, and molecules indeed appear to be the primary cause: the atomic density distributions (not shown) are very similar and, coherently with Figure 15.a, negligibly affected by the change in the reactions in the PFR.
In SOLPS-ITER with its default reactions, molecules are impeded from easily joining and moving in the plasma due to the presence of molecular CX (molecule sink, $\mathrm{D}^+ + \mathrm{D}_2 \rightarrow \mathrm{D} + \mathrm{D}_2^+$) and EL, both absent in SOLEDGE2D. Therefore, in contrast to SOLEDGE2D, a SOLPS-ITER molecule can leave the out-of-plasma inner PFR only by passing through the tiny (~ 8 mm) aperture between the plasma mesh artificial

[9] The origin of red region in the lower portion of the inner PFR is the ion temperature being vanishingly small, as per the atoms in the near-separatrix SOL and at the OMP in Section 5.2.

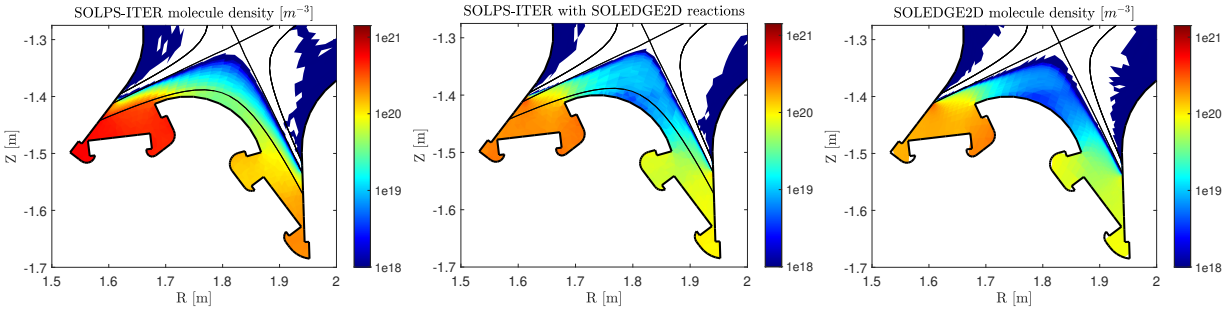

Figure 18: Molecule density in the private-flux region computed by SOLPS-ITER (a), SOLPS-ITER with SOLEDGE2D reactions (b) and SOLEDGE2D (c).

PFR boundary (thin black line in Figure 18) and the divertor dome. Geometrically speaking, this event is unlikely to take place, as justified by the steep radial density gradients closely following the inner portion of the PFR boundary (Figure 18.a). This effect leads, at least partially, to the excess molecular density compared to the SOLEDGE2D inner PFR. However, the artificial nature of the PFR boundary makes the gradients localized along it a SOLPS-ITER artefact. A more open divertor geometry would presumably alleviate this issue, as suggested in [40] where the SOLPS-ITER plasma grid extension in the SOL was varied while the reactions were left unchanged.
The very same dynamics affects the outer PFR as well, but to a lower extent due to the 3.5-times wider PFR-boundary-to-dome aperture ($\sim$ 28 mm) which, along with the bigger radius R, guarantees a larger available volume outside the plasma domain for the molecule to spread. This is supported by the milder (but still observable along the artificial PFR boundary) density gradients in this volume.
Overall, employing SOLEDGE2D reactions also reduces the discrepancy in the absolute magnitudes of the neutral density (pressure) n_g – Section 4.2: the original $4.07 \cdot 10^{21}$ m^{-3} (32.8 Pa) around the inner and the $1.54 \cdot 10^{21}$ m^{-3} (12.7 Pa) around the outer strike point drop to $1.99 \cdot 10^{21}$ m^{-3} (22.9 Pa) and $0.99 \cdot 10^{21}$ m^{-3} (9.9 Pa), respectively, thus more in line with SOLEDGE2D's $1.59 \cdot 10^{21}$ m^{-3} (7.2 Pa) and $0.49 \cdot 10^{21}$ m^{-3} (3.7 Pa).
It is worthwhile noticing that in-out asymmetries, here persisting even after the change in the reactions, have been already observed in experiments and other modelling work [40]. Nonetheless, the SOLPS-ITER plasma mesh not reaching out the divertor wall and SOLEDGE2D not including molecular CX do not allow "extra" molecule sinks (CX itself, EI and DS) which would possibly smooth the asymmetry out.
In regards to UEDGE, its enhanced neutral density in the central PFR and outer strike point can possibly be motivated in terms of the 40% underestimation of DEGAS2 EI (atomic sink) with respect to AMJUEL in the range of temperature and densities characteristic of the PFR (with no notable difference tied to RC processes) [33].

6 Conclusions

This work presents a comparison of the three state-of-the-art edge plasma codes SOLPS-ITER, SOLEDGE2D and UEDGE, employed in modelling a low-power pure-deuterium DTT scenario. Simulations with all codes utilising common magnetic equilibrium, common transport coefficients, common boundary conditions (as far as possible) and a targeted common OMP separatrix electron density (achieved by adjusting the pumping albedo) have been performed, and their results analysed.
Areas of both encouraging agreement and significant disagreement among the code predictions have been identified. For the OMP core, SOLPS-ITER and SOLEDGE2D data are satisfactorily matched, whilst UEDGE deviates from the other two, with an increased plasma density profile and lower temperatures. The opposite discrepancy is observed for UEDGE in the OMP SOL, with a lower density profile and higher electron temperature in the far-SOL. The upstream heat flux width is well matched for all the codes ($\sim$ 8-17%).

Moving downstream to the divertor targets, encouraging agreement is obtained between all the three codes in terms of the peak ion temperatures and outer target parallel heat flux ($\sim$ 1-13%), key design parameters for the divertor. Nevertheless, significant differences are noted also: the outer target peak plasma density is a factor 3-4 lower for SOLEDGE2D compared to the other two codes, UEDGE shows a significantly higher electron temperature in the far-SOL, and SOLPS-ITER displays an inner target parallel heat flux peak lower than the other codes. This disagreement worsens when moving to the PFR, where SOLPS-ITER shows a far PFR ion temperature diverging from SOLEDGE2D's up to a factor 5, although approximately matching UEDGE's. Moreover, the SOLPS-ITER neutral density distribution, despite qualitatively similar to that of SOLEDGE2D in terms of its in-out asymmetric nature, features steep gradients along the artificial PFR boundary, not present in the other codes.

Additional terms intrinsically present in the SOLPS-ITER equations compared to those of SOLEDGE2D and UEDGE are analysed, but found to be of negligible importance in the vast majority of the domain where there is significant plasma density. These terms are therefore considered unlikely to be the cause for the aforementioned discrepancies.

Regarding the OMP differences, the UEDGE assumption of a shared neutral-ion temperature $T_\mathrm{g} = T_\mathrm{i}$ is found to be strongly related to the observed differences, causing a significantly higher puffed neutral penetration into the core that is not observed in the kinetic neutral models. Much better agreement is recovered by UEDGE when reducing T_g to a fraction of T_i, or by limiting the neutral transport, though neither solution appears appropriate for the whole plasma domain. An overall solution may potentially lie in the recently-developed option in UEDGE to individually solve for T_g and T_i [25], but whether the issue is more fundamental to the fluid-vs-kinetic neutral treatment is unclear. Since SOLPS-ITER when run with its fluid neutral model also forces $T_\mathrm{g} = T_\mathrm{i}$ [14], SOLPS-ITER results would presumably be impacted in an analogous manner to the UEDGE results found here.

From the viewpoint of the PFR, the impact of molecules is found to be important, seemingly responsible for both the mild SOLPS-ITER-vs-UEDGE and the substantial SOLPS-ITER-vs-SOLEDGE2D temperature disagreement, due to the absence of molecules in UEDGE simulations and to SOLEDGE2D not currently (but planned to) including the temperature-equilibrating molecule-ion charge exchange nor elastic collisions. The advantage of accounting for these processes in SOLPS-ITER is partially overshadowed by its limited plasma mesh, along with the extended neutral counterpart, resulting in a potential molecular density overestimation in the inner PFR and in density gradients developing along the artificial PFR boundary. In this sense, the new SOLPS-ITER version provided with an extended plasma mesh currently under development would surely be advantageous [46]. Still, both the upgraded SOLPS-ITER and SOLEDGE2D have the potential to further improve by controlling the reactivity values: the computation of the reactivities in a sub-eV-temperature, low-density region, as allowed by an extended plasma mesh, could result in unreasonable values, possibly orders of magnitude away from what one might physically expect, hence partially obscuring the appeal of the extended mesh itself. The same could happen if this is artificially impeded from happening, as can be done in SOLPS-ITER. Thus, a revisitation of the fits to enlarge their validity range may be worthwhile pursuing.

One issue of note arising from the results above relates to the impact on the anomalous transport coefficients. Typical SOL modelling practice commonly consists of (somewhat freely) fine-tuning their radial profile to allow for a close match of simulation output with experimental data. Although it is not the case in the current work (constant coefficients are employed), this provides for the potential to mask both the code-specific limitations discussed above and the physics itself, by differing adjustments of the transport coefficients. This raises potential issues when the codes are used to measure the cross-field transport coefficient values as part of model validation studies. This seems relevant for the UEDGE results, with the higher neutral penetration found in this study impacting both the core and SOL OMP profiles. But, in principle, none of the three codes would be immune to this.

In a more positive perspective, our results highlight, as far as the conditions of the present work allow, the UEDGE capability of reproducing many key variables at the targets, particularly in terms of peak parallel heat flux, plasma density and ion temperature, satisfactorily in agreement with those of the other codes (SOLPS-ITER in particular). This is a noteworthy result given that a primary duty of these codes is providing guidance in the matter of the power exhaust and divertor design. Furthermore, UEDGE could additionally include the full parallel momentum and energy equations for the atoms, and a purely-diffusive neutral molecule transport [25][32], which may further reduce some of the differences found with SOLPS-

ITER and SOLEDGE2D. UEDGE also benefits from an advantage in simulation speed (by a factor 10 or more), with its fully-implicit iteration methods, useful in the context of design studies requiring extensive parameter scans.
Residual persisting differences mainly affecting the SOLEDGE2D results in terms of temperature onset at both targets and peak plasma density at outer target if compared to the other codes are planned to be investigated in the future. Possible causes of such discrepancies are presumably attributed to the SOLEDGE2D extended mesh, not present in the other two codes.
In addition to this, further cross-code comparison studies aimed at modelling a full-power neon-seeded DTT scenario and an H-mode DTT-relevant Alcator C-Mod plasma discharge are currently ongoing, to compare the predictions of the codes in a highly-radiative, detached divertor regime, and their ability to reproduce experimental data.

Acknowledgements

This work was made possible with fellowship support from Eni S.p.A. through the MIT Energy Initiative and is funded by Eni S.p.A., contract n. 4310369990, in the framework of a 4-Ways Agreement between Eni, MIT, CFS and ENEA. The authors acknowledge the support of the SOLPS-ITER, SOLEDGE2D and UEDGE teams, especially of X. Bonnin for his precious pieces of advice in the matter of SOLPS-ITER, and of M. Umansky and T. Rognlien for their useful discussions in support of the UEDGE work.

Appendices

A Magnetic equilibrium reconstruction issues

The present appendix concerns issues detected in SOLEDGE2D, but possibly affecting edge plasma codes more generally, in the process of the mesh creation (Section 3.1) from the magnetic equilibrium, to allow the mesh cells to be as aligned as possible (along x) to magnetic surfaces.
A first mesh (smooth mesh) is generated by carrying out a smoothing procedure, consisting in applying a bivariate spline over the equilibrium with a smoothing factor of 1 % [47] to help the grid generator finding the position of magnetic nulls and avoiding cell misalignment. The second mesh (non-smooth mesh) is instead created by avoiding such process. Figure 19 pictures the SOLEDGE2D separatrix in both cases, with and without smoothing: the disagreement in the divertor region results in a few-cell misalignment of the strike points on the targets, with a corresponding linear difference of 4 mm at outer target and 28 mm at inner target. As a consequence of this misalignment, the value of the connection length $L_{\parallel}$ and of the grazing angle ϑ change up to 15%.
SOLEDGE2D is then run by alternatively employing both meshes, but with exactly the same remaining input settings (as for Section 3). The reference SOLEDGE2D results discussed throughout Sections 4 and 5 rely on the non-smooth mesh, which matches that of SOLPS-ITER and UEDGE. According to Figure 20, an overall significant sensitivity to the magnetic equilibrium details is found in terms of both plasma and neutral parameters in the divertor region.
In terms of the molecule density, changing from the smooth to the non-smooth mesh implies the density distribution, initially in-out symmetric in a UEDGE-like fashion (Figure 4.c), acquiring a strong asymmetry, close to that observed in SOLPS-ITER and commented in Section 5.6. The plasma density at the divertor targets features a qualitatively similar trend, with the overall maximum density attained at outer target with smooth mesh remarkably decreasing of a factor 2.5-3 in favour of a parallel growth on the opposite target with non-smooth mesh. Finally, the peak perpendicular heat flux at inner target changes by 25%. This picture is consistent with a power redistribution occurring between the targets, with the leading cause behind this presumably lying in the modifications occurring for the abovementioned connection length and grazing angle.

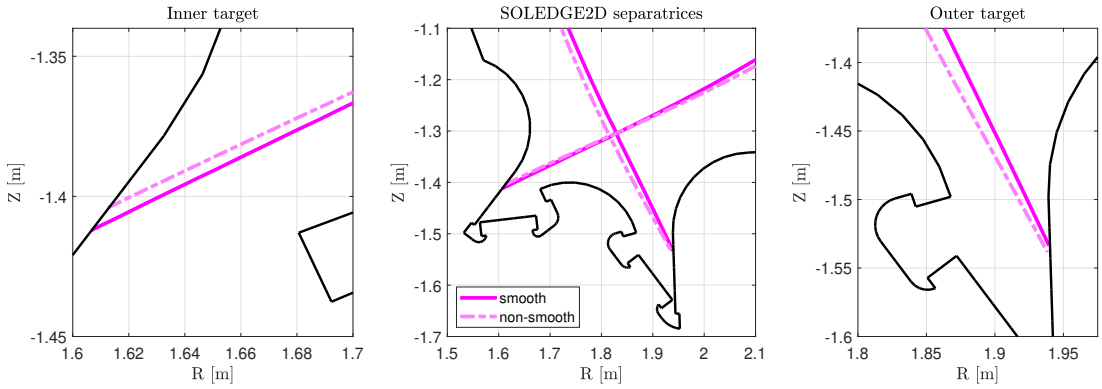

Figure 19: SOLEDGE2D separatrices with smooth and non-smooth mesh.

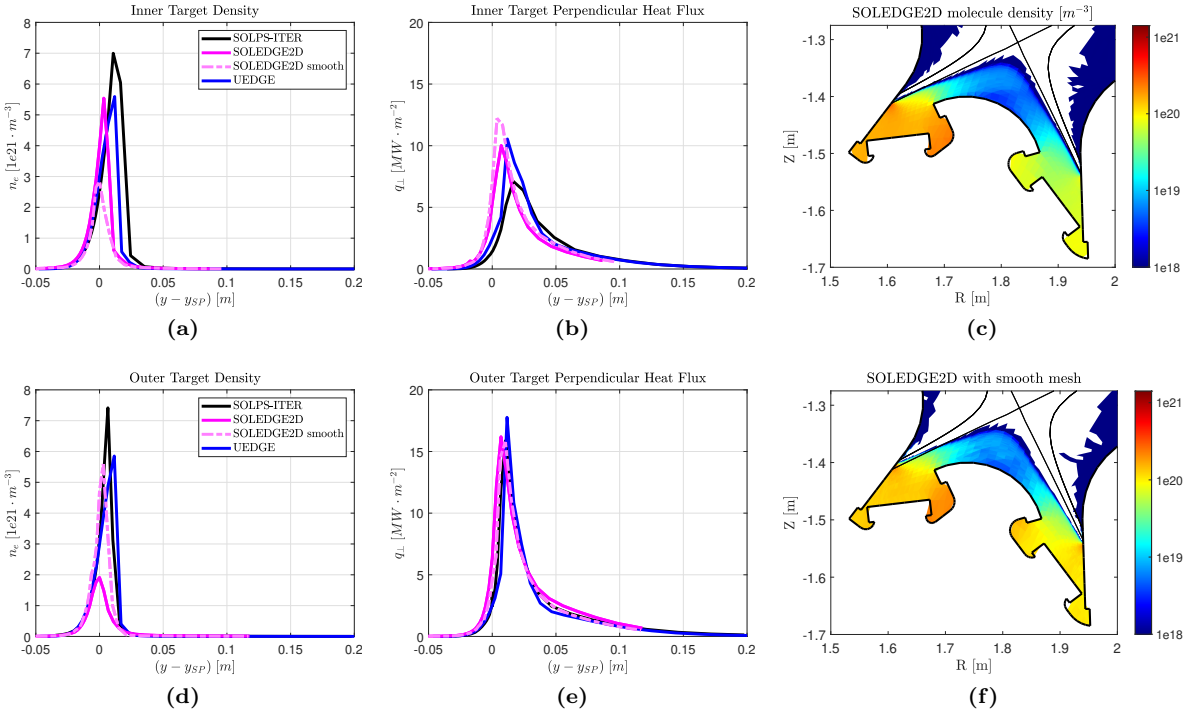

Figure 20: Comparison of SOLEDGE2D with smooth and with non-smooth (Sections 4 and 5) mesh against SOLPS-ITER and UEDGE reference results. Inner target (a and b) and outer target (d and e) density and perpendicular heat flux. c and f picture SOLEDGE2D molecule density with non-smooth and smooth mesh, respectively.

References

[1] A.J.H. Donné. 'The European roadmap towards fusion electricity'. In: *Philosophical Transactions of the Royal Society A* 377 (2019), p. 2141.

[2] G. Federici, C. Bachmann, L. Barucca and W. Biel et al. 'DEMO design activity in Europe: Progress and updates'. In: *Fusion Engineering and Design* 136 (2018), pp. 729–741. DOI: https://doi.org/10.1016/j.fusengdes.2018.04.001.

[3] B.N. Sorbom, J. Ball, T.R. Palmer and F.J. Mangiarotti et al. 'ARC: A compact, high-field, fusion nuclear science facility and demonstration power plant with demountable magnets'. In: *Fusion Engineering and Design* 100 (2015), pp. 378–405. DOI: https://doi.org/10.1016/j.fusengdes.2015.07.008.

[4] T. Eich, A.W. Leonard, R.A. Pitts and W. Fundamenski et al. 'Scaling of the tokamak near the scrape-off layer H-mode power width and implications for ITER'. In: *Nuclear Fusion* 53.9 (2013), p. 093031. DOI: 10.1088/0029-5515/53/9/093031.

[5] T. Eich, P. Manz, R.J. Goldston, P. Hennequin and P. David et al. 'Turbulence driven widening of the near-SOL power width in ASDEX Upgrade H-Mode discharges'. In: *Nuclear Fusion* 60.5 (2020), p. 056016. DOI: 10.1088/1741-4326/ab7a66.

[6] G.F. Nallo, G. Mazzitelli, L. Savoldi, F. Subba and R. Zanino. 'Self-consistent modelling of a liquid metal box-type divertor with application to the divertor tokamak test facility: Li versus Sn'. In: *Nuclear Fusion* 59.6 (2019), p. 066020. DOI: 10.1088/1741-4326/ab145b.

[7] S. Wiesen, M. Groth, M. Wischmeier and S. Brezinsek et al. 'Plasma edge and plasma-wall interaction modelling: Lessons learned from metallic devices'. In: *Nuclear Materials and Energy* 12 (2017), pp. 3–17. DOI: https://doi.org/10.1016/j.nme.2017.03.033.

[8] G.F. Nallo, G. Mazzitelli, M. Moscheni, F. Subba and R. Zanino. 'SOLPS-ITER simulations of a CPS-based liquid metal divertor for the EU DEMO: Li vs. Sn'. In: *submitted to Nuclear Fusion* (2021).

[9] F. Militello, L. Aho-Mantila, R. Ambrosino and T. Body et al. 'Preliminary analysis of alternative divertors for DEMO'. In: *Nuclear Materials and Energy* 26 (2021), p. 100908. DOI: https://doi.org/10.1016/j.nme.2021.100908.

[10] M.R.K. Wigram, B. LaBombard, M.V. Umansky and A.Q. Kuang et al. 'Performance assessment of long-legged tightly-baffled divertor geometries in the ARC reactor concept'. In: *Nuclear Fusion* 59 (2019), p. 106052. DOI: 10.1088/1741-4326/ab394f.

[11] F. Subba, L. Aho-Mantila, D. Coster and G. Maddaluno et al. 'Modelling of mitigation of the power divertor loading for the EU DEMO through Ar injection'. In: *Plasma Physics and Controlled Fusion* 60.3 (2018), p. 035013. DOI: 10.1088/1361-6587/aaa508.

[12] A. Kallenbach, M. Bernert, R. Dux and L. Casali et al. 'Impurity seeding for tokamak power exhaust: from present devices via ITER to DEMO'. In: *Plasma Physics and Controlled Fusion* 55.12 (2013), p. 124041. DOI: 10.1088/0741-3335/55/12/124041.

[13] R. Martone, R. Albanese, F. Crisanti, A. Pizzuto and P. Martin. 'Eds. DTT Divertor Test Tokamak Facility Interim Design Report'. In: (2019). URL: https://www.dtt-dms.enea.it/share/s/avvglhVQT2aSkSgV9vuEtw.

[14] X. Bonnin, W. Dekeyser, R. Pitts and D. Coster et al. 'Presentation of the New SOLPS-ITER Code Package for Tokamak Plasma Edge Modelling'. In: *Plasma and Fusion Research* 11 (2016), pp. 1403102–1403102. DOI: 10.1585/pfr.11.1403102.

[15] H. Bufferand, C. Baudoin, J. Bucalossi and G. Ciraolo et al. 'Implementation of drift velocities and currents in SOLEDGE2D–EIRENE'. In: *Nuclear Materials and Energy* 12 (2017), pp. 852–857. DOI: https://doi.org/10.1016/j.nme.2016.11.031.

[16] T.D. Rognlien, J.L. Milovich, M.E. Rensink and G.D. Porter. 'A fully implicit, time dependent 2-D fluid code for modeling tokamak edge plasmas'. In: *Journal of Nuclear Materials* 196-198 (1992), pp. 347–351. DOI: https://doi.org/10.1016/S0022-3115(06)80058-9.

[17] L. Owen, T.D. Rognlien, G.D. Porter, X. Bonnin and D. Coster. 'Benchmarking the UEDGE and SOLPS edge plasma transport codes in DIII-D and JET geometries.' In: *Bulletin of the American Physical Society* (2006).

[18] N. Rivals et al. In: (2021). Submitted to Contributions to Plasma Physics.

[19] A.V. Chankin and D.P. Coster. 'Comparison of 2D models for the plasma edge with experimental measurements and assessment of deficiencies'. In: *Journal of Nuclear Materials* 390-391 (2009), pp. 319–324. DOI: https://doi.org/10.1016/j.jnucmat.2009.01.307.

[20] R Balescu. *Transport processes in plasmas. Pts. 1 and 2*. 1988.

[21] V. Zhdanov. *Transport processes in multicomponent plasma*. New York, London: Taylor and Francis, 2002.

[22] T. D. Rognlien, D. D. Ryutov, N. Mattor and G. D. Porter. 'Two-dimensional electric fields and drifts near the magnetic separatrix in divertor tokamaks'. In: *Physics of Plasmas* 6.5 (1999), pp. 1851–1857. DOI: 10.1063/1.873488.

[23] V.A Rozhansky, S.P Voskoboynikov, E.G Kaveeva, D.P Coster and R Schneider. 'Simulation of tokamak edge plasma including self-consistent electric fields'. In: *Nuclear Fusion* 41.4 (2001), pp. 387–401. DOI: 10.1088/0029-5515/41/4/305.

[24] M. Itskov. *Tensor Algebra and Tensor Analysis for Engineers: With Applications to Continuum Mechanics*. 2nd. Springer Publishing Company, Incorporated, 2009. ISBN: 3540939067.

[25] M. Zhao, A.E. Jaervinen, I. Joseph and T.D. Rognlien. 'Impact of ion temperature anisotropy on 2D edge-plasma transport'. In: *Nuclear Materials and Energy* 26 (2021), p. 100881. DOI: https://doi.org/10.1016/j.nme.2020.100881.

[26] S. Togo, T. Takizuka, D. Reiser and K. et al. Hoshino. 'Study of mirror effect on scrape-off layer-divertor plasma based on a generalized fluid model incorporating ion temperature anisotropy'. In: *Contributions to Plasma Physics* 58.6-8 (2018), pp. 556–562. DOI: https://doi.org/10.1002/ctpp.201700170.

[27] D. Reiter. *The EIRENE Code User Manual*. 2019. URL: http://www.eirene.de/eirene.pdf.

[28] J.P. Freidberg. *Plasma Physics and Fusion Energy*. Cambridge University Press, 2007. DOI: 10.1017/CBO9780511755705.

[29] D. Reiter. *The data file AMJUEL: Additional Atomic and Molecular Data for EIRENE*. 2020. URL: http://www.eirene.de/html/amjuel.html.

[30] D. Reiter. *The data file HYDHEL: Atomic and Molecular Data for EIRENE*. 2020. URL: http://www.eirene.de/html/hydhel.html.

[31] P.C. Stangeby. *The Plasma Boundary of Magnetic Fusion Devices*. Series in Plasma Physics and Fluid Dynamics. Taylor & Francis, 2000. ISBN: 9780750305594. URL: https://books.google.co.uk/books?id=qOliQgAACAAJ.

[32] T.D. Rognlien, M.E. Rensink and D.P. Stotler. 'Scrape-off layer plasma and neutral characteristics and their interactions with walls for FNSF'. In: *Fusion Engineering and Design* 135 (2018), pp. 380–393. DOI: https://doi.org/10.1016/j.fusengdes.2017.07.024.

[33] D. Stotler, C. Karney, R. Kanzleiter and S. Jaishankar. 'User's Guide for DEGAS2 (Release V. 4.9)'. In: (2019). URL: https://w3.pppl.gov/degas2/.

[34] P. Helander, S.I. Krasheninnikov and P.J. Catto. 'Fluid equations for a partially ionized plasma'. In: *Physics of Plasmas* 1.10 (1994), pp. 3174–3180. DOI: 10.1063/1.870470.

[35] S. I. Braginskii. 'Transport Processes in a Plasma'. In: 1 (1965), pp. 205–311.

[36] R. Schneider and A Runov. 'Challenges in plasma edge fluid modelling'. In: *Plasma Phys. Control. Fusion* 49 (2007), pp. 87–95. DOI: 10.1088/0741-3335/49/7/S06.

[37] M.R.K. Wigram, C.P. Ridgers, B.D. Dudson, J.P. Brodrick and J.T. Omotani. 'Incorporating non-local parallel thermal transport in 1D ITER SOL modelling'. In: *Nuclear Fusion* 60 (2020), p. 076008. DOI: 10.1088/1741-4326/ab868b.

[38] D. Brunner, B. LaBombard, R.M. Churchill and J. Hughes et al. 'An assessment of ion temperature measurements in the boundary of the Alcator C-Mod tokamak and implications for ion fluid heat flux limiters'. In: *Plasma Physics and Controlled Fusion* 55.9 (2013), p. 095010. DOI: 10.1088/0741-3335/55/9/095010.

[39] R. Albanese, R. Ambrosino and M. Mattei. 'CREATE-NL+: A robust control-oriented free boundary dynamic plasma equilibrium solver'. In: *Fusion Engineering and Design* 96-97 (2015), pp. 664–667. DOI: https://doi.org/10.1016/j.fusengdes.2015.06.162.

[40] S. Wiesen, S. Brezinsek, X. Bonnin and E. et al. Delabie. 'On the role of finite grid extent in SOLPS-ITER edge plasma simulations for JET H-mode discharges with metallic wall'. In: *Nuclear Materials and Energy* 17 (2018), pp. 174–181. DOI: 10.1016/j.nme.2018.10.013.

[41] R.J. Goldston, M.L. Reinke and J.A. Schwartz. 'A new scaling for divertor detachment'. In: *Plasma Physics and Controlled Fusion* 59.5 (2017), p. 055015. DOI: 10.1088/1361-6587/aa5e6e.

[42] S.I. Krasheninnikov and A.S. Kukushkin. 'Physics of ultimate detachment of a tokamak divertor plasma'. In: *Journal of Plasma Physics* 83.5 (2017), p. 155830501. DOI: 10.1017/S0022377817000654.

[43] F. Subba, D.P. Coster, M. Moscheni and M. Siccinio. 'SOLPS-ITER modeling of divertor scenarios for EU-DEMO'. In: 61.10 (2021), p. 106013. DOI: 10.1088/1741-4326/ac1c85.

[44] E. Havlíčková, W. Fundamenski, M. Wischmeier, G. Fishpool and A.W. Morris. 'Investigation of conventional and Super-X divertor configurations of MAST Upgrade using scrape-off layer plasma simulation'. In: *Plasma Physics and Controlled Fusion* 56.7 (2014), p. 075008. DOI: 10.1088/0741-3335/56/7/075008.

[45] K. Ghoos, P. Boerner, W. Dekeyser, A. Kukushkin and M. Baelmans. 'Grid resolution study for B2-EIRENE simulation of partially detached ITER divertor plasma'. In: *Nuclear Fusion* 59 (2018). DOI: 10.1088/1741-4326/aaf30f.

[46] W. Dekeyser, P. Boerner, S. Voskoboynikov and V.A. Rozhanksy et al. 'Plasma edge simulations including realistic wall geometry with SOLPS-ITER'. In: *Nuclear Materials and Energy* 27 (2021), p. 100999. DOI: https://doi.org/10.1016/j.nme.2021.100999.

[47] Bivariate spline, Scipy (Python). URL: https://docs.scipy.org/doc/scipy/reference/generated/scipy.interpolate.RectBivariateSpline.html.